

TNO report
PML 1998-A38

**Dynamic deformation capacity of reinforced
concrete.
Phase 5: influence of lacing reinforcement**

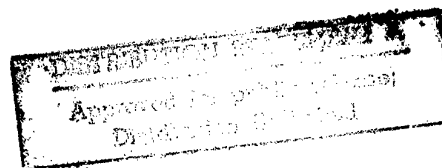
TNO Prins Maurits Laboratory

Lange Kleiweg 137
P.O. Box 45
2280 AA Rijswijk
The Netherlands

Phone +31 15 284 28 42
Fax +31 15 284 39 58

Date
December 1998

Author(s)
J.C.A.M. van Doormaal
S. Caron



Reproduced From
Best Available Copy

Classification
Classified by : D. Boon
Classification date : 3 November 1998
(This classification will not change)

Title : Ongerubriceerd
Managementuitreksel : Ongerubriceerd
Abstract : Ongerubriceerd
Report text : Ongerubriceerd
Annexes A - D : Ongerubriceerd

19990112 086

All rights reserved.
No part of this publication may be reproduced and/or published by print, photoprint, microfilm or any other means without the previous written consent of TNO.

In case this report was drafted on instructions from the Ministry of Defence the rights and obligations of the principal and TNO are subject to the standard conditions for research and development instructions, established by the Ministry of Defence and TNO, if these conditions are declared applicable, or the relevant agreement concluded between the contracting parties.

Copy no. : 14
No. of copies : 26
No. of pages : 64 (incl. annexes,
excl. RDP & distribution list)
No. of annexes : 4

All information which is classified according to Dutch regulations shall be treated by the recipient in the same way as classified information of corresponding value in his own country. No part of this information will be disclosed to any party.

The classification designation Ongerubriceerd is equivalent to Unclassified.

© 1998 TNO

TNO Prins Maurits Laboratory is part of
TNO Defence Research which further consists of:

TNO Physics and Electronics Laboratory
TNO Human Factors Research Institute



AQF99-04-0586

Netherlands Organization for
Applied Scientific Research (TNO)

Managementuittreksel

Titel : Dynamic deformation capacity of reinforced concrete.
Phase 5: influence of lacing reinforcement
Auteur(s) : Ir. J.C.A.M. van Doormaal, S. Caron
Datum : december 1998
Opdrachtnr. : A96D449
Rapportnr. : PML 1998-A38

In het kader van de door MOD-NL/DWOO/HWO-CO geplaatste opdracht A96D449 zijn in overleg met de projectbegeleider schokgolffexperimenten uitgevoerd op vrij opgelegde platen van gewapend beton. Tijdens deze experimenten is de weerstand-vervormingskarakteristiek van de geteste panelen bepaald en daaruit is de vervormingscapaciteit van de platen afgelezen. De aandacht ging met name uit naar de invloed van veterwapening op de vervormingscapaciteit. De huidige proevenserie is een vervolg op eerdere experimenten ([1], [2] en [3]), waarin eveneens de dynamische vervormingscapaciteit van het gewapende beton onderwerp van onderzoek was.

De aanleiding om onderzoek te doen naar deze grootheid was de observatie dat in ontwerpvoorschriften vaak conservatieve waarden voor de toelaatbare vervorming van gewapend beton worden voorgeschreven. Conservatisme is uiteraard onvermijdelijk voor ontwerpvoorschriften die algemeen toepasbaar moeten zijn. Maar aan het conservatieve karakter van de voorschriften ten aanzien van de toelaatbare vervorming van gewapend beton blijkt ook een hiaat in kennis ten grondslag te liggen. Dit betekent dat beschermingsconstructies vaak economischer ontworpen kunnen worden of dat beschermingsconstructies een hogere beschermingsgraad hebben dan wordt aangenomen. Om deze wetenschap te kunnen benutten is een beter begrip ten aanzien van de dynamische vervormingscapaciteit en de invloedsparameters nodig.

De voorgaande experimenten hebben reeds waardevolle resultaten opgeleverd. Het bleek mogelijk om een empirische relatie te formuleren tussen de testparameters en de vervormingscapaciteit van de plaat. Omdat deze empirische relatie gebaseerd was op een beperkt aantal testen, is uitgebreidere validatie nodig.

Een onverwacht, en tevens alarmerend, resultaat was gevonden voor betonplaten met veterwapening (het zogenaamde 'lacing'). TM 5-1300 bleek in deze situatie niet conservatief, integendeel zelfs: TM 5-1300 bleek onveilig. Een goede verklaring voor het onverwachte resultaat was niet gevonden. Daarom is de huidige serie experimenten op dikkere platen uitgevoerd met de aandacht op de invloed van veterwapening op de vervormingscapaciteit.

De experimenten zijn uitgevoerd met behulp van vier explosieve ladingen, die gezamenlijk een nagenoeg uniform verdeelde belasting zouden moeten genereren. Dit is een andere opstelling dan in de voorgaande testseries is gebruikt, waar de

belasting werd gegenereerd met de schokgolfsimulator van het TNO Prins Maurits Laboratorium (TNO-PML). Deze wijziging in opstelling, die noodzakelijk was vanwege de beperkingen van de schokgolfsimulator, geeft de mogelijkheid om te controleren of de duur van de schokgolf invloed heeft op de respons-mode van de betonplaat.

De doelstelling van de huidige serie experimenten is:

- uitbreiding of begrenzing van de toepasbaarheid van de eerder gevonden empirische relatie;
- invloed van 'lacing' op de vervormingscapaciteit van gewapend beton;
- vergelijking tussen de 'response mode' onder een nucleaire schokgolf en de schokgolf van een 'high explosive'.

Een zevental platen zijn getest in het reactieframe van het TNO-PML in de bunker van het Laboratorium voor Ballistisch Onderzoek. Deze platen waren op twee verschillende wijzen gewapend op buiging en bevatten al dan niet lacing om de invloed daarvan te onderzoeken.

Ondanks diverse problemen met de nieuwe opstelling kon de weerstand-vervormingscurve bepaald worden en daaruit ook de vervormingscapaciteit. Dit leidde tot de volgende conclusies.

- De resultaten sluiten aan bij de voorgaande resultaten. Het impulsieve karakter van de belasting verandert het gedrag van de plaat niet.
- De eerder gevonden empirische relatie blijkt geldig mits falen ten gevolge van knik van de wapening in de drukzone optreedt.
- De vervormingscapaciteit neemt toe met de diameter van de buigwapening.
- 'Lacing' verhoogt de vervormingscapaciteit alleen als anders het knikken van de drukwapening falen zou inleiden.
- Een nieuwe empirische relatie is gevonden als breuk van de trekwapening tot falen leidt.
- Wees voorzichtig bij het toepassen van de ontwerpvoorschriften in TM 5-1300 voor platen met veterwapening.

De combinatie van beide empirische relaties geeft een methode om de toelaatbare vervorming van gewapende betonnen platen te bepalen, zowel economisch als veilig. Het geeft inzicht in de faalmode van de plaat.

De geldigheid van de empirische relaties is slechts beperkt geverifieerd. Daarom zijn meer testen nodig, waarbij nog niet gevarieerde parameters ook in beschouwing moeten worden genomen. Het is echter raadzaam om voor het uitvoeren van nieuwe testen de testopstelling nog eens grondig te bestuderen en te verbeteren. De parameterstudie moet zich niet beperken tot enkel experimenteel onderzoek. Het aantal experimenten kan beperkt worden door de experimenten te combineren met numerieke simulaties.

Contents

Managementuittreksel	2
1 Introduction	5
2 Experimental programme	7
2.1 Introduction	7
2.2 The slabs	7
2.3 Test set-up	12
2.4 Test programme	13
2.5 Measurements	14
3 Results	16
3.1 Introduction	16
3.2 Problems	16
3.3 Approach for determining the resistance-deformation curve	17
3.4 Test 1 - Slab 7	18
3.5 Tests 2 and 3 - Slab 3	20
3.6 Test 4 - slab 4	24
3.7 Test 5+6 - Slab 6	27
3.8 Test 7 - Slab 1	29
3.9 Test 8 - Slab 2	32
3.10 Test 9+10 - Slab 5	35
4 Discussion of results	38
4.1 Introduction	38
4.2 Comparison of the present tests	38
4.3 Comparison with TM 5-1300 calculations	39
4.4 Comparison of the results with previous test results	39
4.5 Criterion for tensile failure	41
4.6 Discussion of the test method	43
5 Conclusions	45
6 References	47
7 Authentication	48
Annexes	
A Concrete composition	
B Calculations and predictions	
C Shock load	
D Manipulation of the measured signals	

1 Introduction

On behalf of MOD-NL/DWOO/HWO-CO, blast experiments were carried out on simply supported reinforced concrete slabs in order to determine their resistance-deformation characteristic up to failure. These tests were performed using explosive charges. The main interest was the dynamic rotation capacity of the slabs and the influence of lacing reinforcement on this rotation capacity.

The present test series is a sequel to previous test series ([1], [2] and [3]), in which the dynamic rotation capacity of reinforced concrete slabs was also the main subject. The interest in the dynamic deformation capacity has been raised by the observation that in design rules, often conservative values are used for the ultimate deformation capacity of reinforced concrete (see [4]). That means that the protection level of concrete structures is often higher than assumed. In order to be able to turn this knowledge to profit, a better understanding of the dynamic deformation capacity and of the parameters of influence are needed.

The previous tests have given valuable results. It appeared to be possible to formulate an empirical relationship between the test parameters and the deformation capacity of the slab. This relationship is for slabs without tying reinforcement. Since this empirical relationship is only based on a limited number of tests, its validity is proven only limitedly. Therefore, more validation would be welcome. For slabs with tying reinforcement, especially lacing, unexpected results were obtained. The deformation capacity did not increase as much as expected based on the design rules of TM 5-1300 [5]. Instead of a higher value for the deformation capacity, a lower value was found. That means that the design rules are not conservative, but on the contrary, unsafe.

A good explanation was not found for the small deformation capacity of the laced slabs. Therefore a new set of experiments has been performed in order to get more insight into the influence of lacing on the deformation capacity. Thicker slabs were chosen because the dimensions are more realistic for protective structures, i.e. the type of structures for which TM 5-1300 has been developed.

An advantage of thicker slabs is that it makes it possible to extend the validity of the empirical formula or to demarcate it.

A disadvantage, however, is that the capacity of the blast simulator is not sufficient to bring these slabs to failure. This problem was encountered in previous tests.

Another test set-up was therefore chosen. The slabs were loaded by detonating explosive charges. Whereas the test set-up in the blast simulator was known very well and therefore well under control, we did not have much experience with this new set-up; new problems may arise and have to be solved.

On the other hand, the use of explosive charges changes the character of the loading to more impulsive. The response and therefore the failure mode might be different. The present test series gives the opportunity to check whether the previous results will also be valid under a more impulsive load, resulting from the detonation of explosives.

ous results will also be valid under a more impulsive load, resulting from the detonation of explosives.

The objectives of the present test series are:

- expansion or demarcation of the empirical relationship, found in the previous tests;
- influence of lacing on the deformation capacity of reinforced concrete;
- comparison of the response mode under nuclear blast and impulsive shock load.

In this report, the experiments and the results are described. In Chapter 2, the experimental programme is given. All data on the slabs is presented in this chapter. Furthermore, a description of what is measured during the tests is given. Chapter 3 gives the results of each slab tested in the present programme. The behaviour of each slab is described with the use of the resistance-deformation curve obtained from the measurements.

In Chapter 4, the results of the tests are compared with each other and with the results of the previous test programme. They are also compared with calculations according to TM 5-1300 [5].

The report ends with Chapter 5 with all the conclusions of the research project.

2 Experimental programme

2.1 Introduction

The slabs in the present programme were tested in a different set-up than in the previous programmes. This has to do with the capacity of the blast simulator, which is not sufficient for the slabs which were tested now.

Other differences between the present programme and the previous ones concerned the thickness of the slab and the diameter of the longitudinal reinforcement.

An overview of the test programme is given in this chapter. Furthermore, a description of the slabs and the test set-up is given. The principle of the test method is the same. The reader is referred to reference [1] for that.

2.2 The slabs

The primary objective of the test programme was to get a better understanding of the influence of lacing on the deformation capacity of reinforced concrete. Therefore it was decided to test both slabs with only bending reinforcement as a reference and the same slabs but with lacing. Two different reference slabs were chosen. In total four types of slabs were tested.

- Type 4.1.1: reference slab 1 without lacing;
- Type 4.1.2: similar to type 4.1.1 but with lacing;
- Type 4.2.1: reference slab 2 without lacing;
- Type 4.2.2: similar to type 4.2.1 but with lacing.

The numbering of the slabs is a sequel to the numbering of the previous test series. Number 4 means that this is the fourth test series. The second number refers to the two reference slabs in this test series. The third number refers to whether the slab contains lacing or not (1 is no lacing, 2 is with lacing).

All slabs were 125 mm thick, which is thicker than the 70 to 100 mm thick slabs in the previous test series.

Other parameters were kept the same as much as possible, i.e. the reinforcement ratio and the quality of both concrete and steel. This made it possible to compare the results with the previous results.

In Table 2.1, Figures 4.1, 4.2 and 4.3, all data on the dimensions of the slabs and the material properties are presented. One is referred to Annex A for more information about the concrete.

Table 2.2 gives the numbering and the type of the slabs.

The lacing reinforcement of the slabs was designed according to the rules of TM 5-1300. This lacing reinforcement looked a bit different for both types of slabs. For

slab type 4.1.2, lacing method no. 1 in TM 5-1300 is used, similarly as for slab type 3.3 of the previous test series, i.e. a single zigzag reinforcement bar per longitudinal bar. For slab type 4.2.2, this would have resulted in too thick reinforcement bars for the lacing. It would have been too difficult to bend the bars. Therefore, lacing method no. 2 of TM 5-1300 was applied, for this slab type, i.e. two zigzag lacing bars per longitudinal bar.

Table 2.1: Data on tested slabs.

	Slab type 4.1	Slab type 4.2
Dimensions of slabs		
Length L [mm]	1200	1200
Support length L _s [mm]	1100	1100
Width W [mm]	850	850
Height H [mm]	125	125
Mass M _{tot} (*) [kg]	294.6	294
Reinforcement		
Diameter ϕ [mm]: longitudinal reinforcement	8	10
Diameter ϕ [mm]: transversal reinforcement	8	8
In-between distance b [mm]	130	175
Concrete cover c [mm]	15	15
Number of rods	7	5
Ratio [%]	0.0422	0.0476
Properties of concrete		
Cube strength f_c [MPa]	48.6	48.6
Young's modulus E_c [GPa]	29.6	29.6
Poisson's ratio ν	0.167	0.167
Properties of steel		
Yield's strength f_y [MPa]	500	500
Ultimate strength f_u [MPa]	580	580
Young's modulus E_s [GPa]	210	210

(*) Mass M_{tot} is the mass of the slabs without lacing. The slabs with lacing were not weighed, since the mass of the lacing reinforcement amounts to less than 2 kg, which is negligible in comparison with the global mass.

Table 2.2: Numbering of slabs.

Slab number	Lacing	Longitudinal reinforcement	Type
1	yes	5 bars of 10 mm	type 4.2.2
2	no	5 bars of 10 mm	type 4.2.1
3	yes	7 bars of 8 mm	type 4.1.2
4	yes	7 bars of 8 mm	type 4.1.2
5	no	7 bars of 8 mm	type 4.1.1
6	no	7 bars of 8 mm	type 4.1.1
7	no	7 bars of 8 mm	type 4.1.1

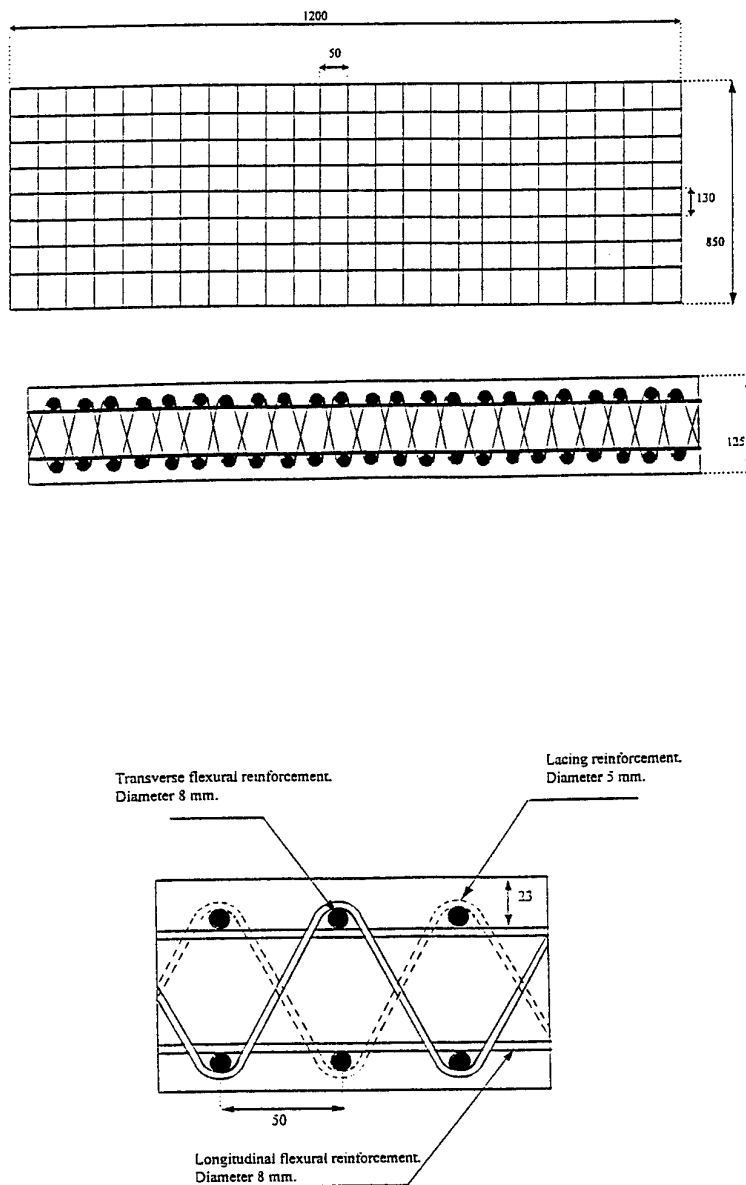


Figure 2.1: Dimensions and distribution of reinforcement in slabs of type 4.1.2. (dimensions in mm).

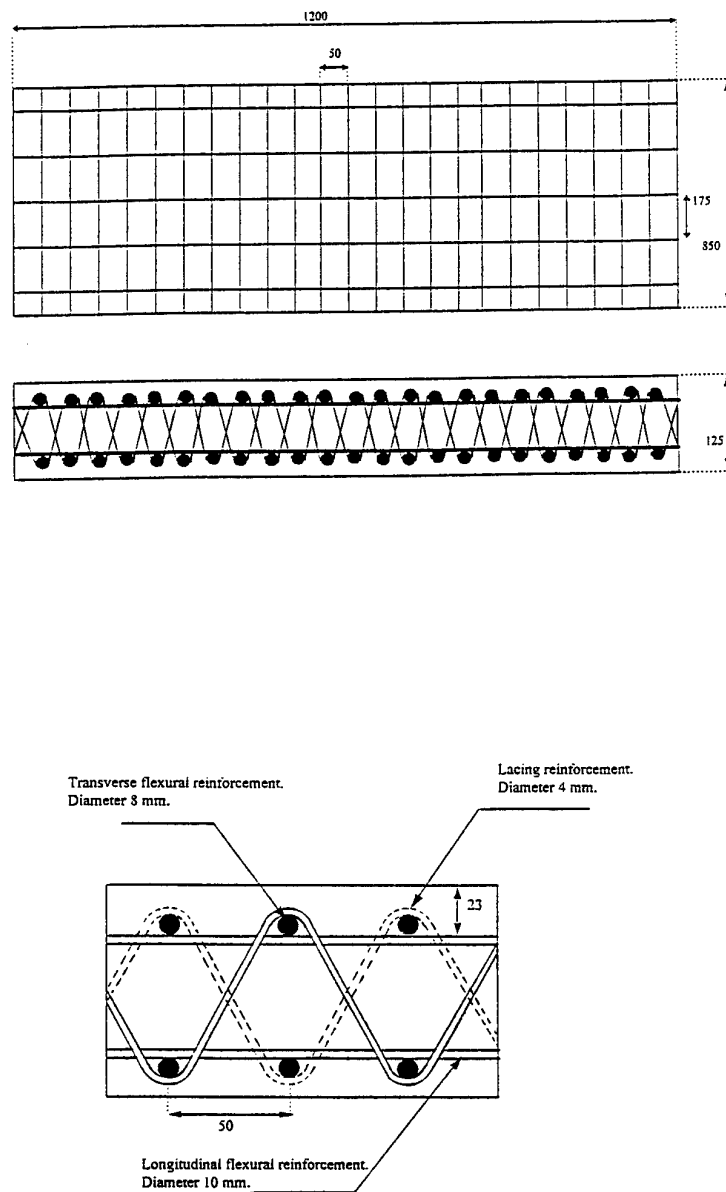


Figure 2.2: Dimensions and distribution of reinforcement in slabs of type 4.2.2. (dimensions in mm).

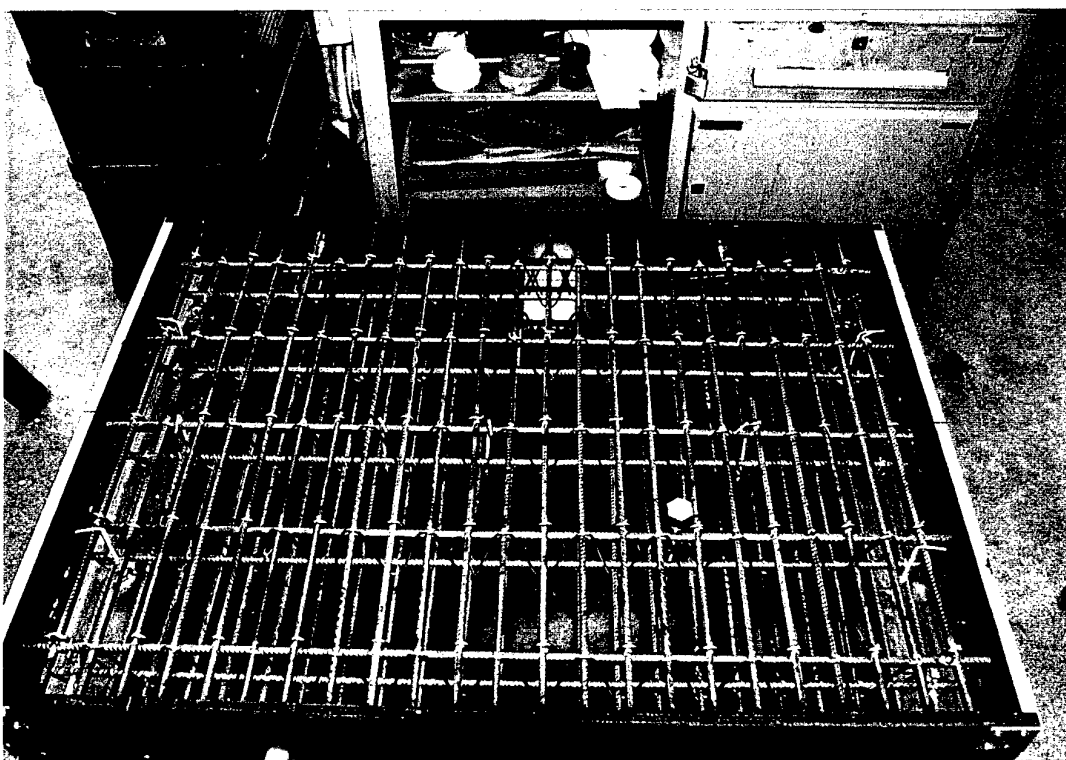
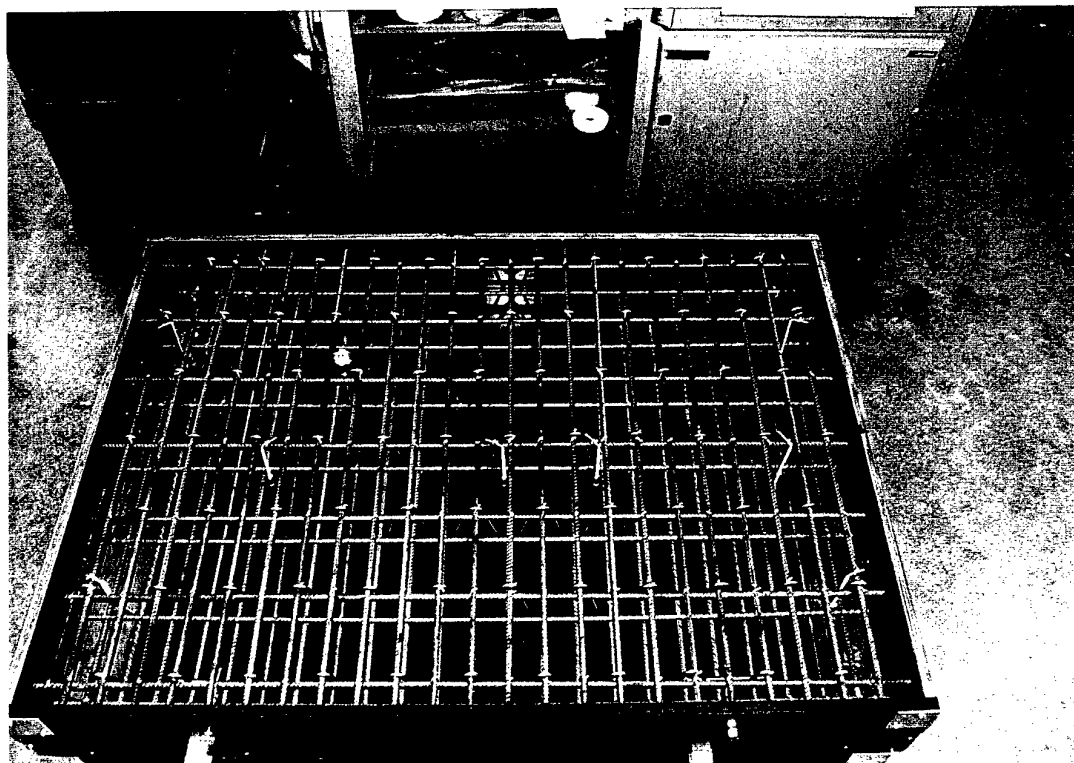


Figure 2.3: Picture of laced slabs, type 4.1.2 and type 4.2.2.

2.3 Test set-up

The tests were performed in the LBO bunker of TNO-PML, where it is allowed to detonate up to 25 kg of TNT. The slab was placed in a horizontal position on a reaction frame, which was especially designed to sustain high loads such as blast loads of explosive materials.

For comparison reasons, the fixation of the slab was kept the same as in the test set-up in the blast simulator, i.e. the slab was lightly clamped between a steel roller on the unloaded side and a layer of rubber on the loaded side. An additional advantage of this fixation is that in case of rebound, the slab would be kept in place. The whole set-up is drawn in Figure 2.4.

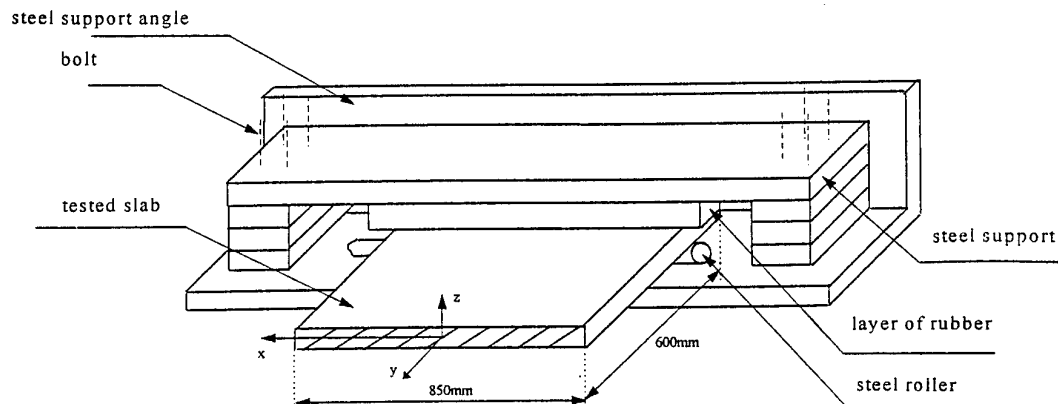


Figure 2.4: Perspective of the half test set-up.

The dynamic load was applied to the slab by detonating four charges simultaneously above the slab. According to [6] this would give approximately a uniform pressure distribution. KNEED no. 6 (a plastic explosive) was used for the explosion.

The positions of the four charges were determined by analogy with the experimental results in reference [6]. These positions only depend on the dimensions of the slab. They are shown in Figure 2.5.

Figure 2.6 shows the complete test set-up with the four charges. The charges are suspended above the slab by means of small bent iron bars welded on the steel support. These bars are believed to be blown away by the explosion and, consequently, they should not hit the concrete slab. The experiments proved this was sufficient.

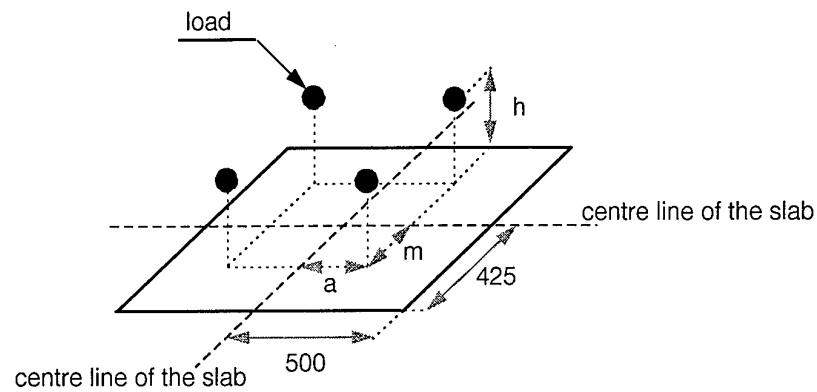


Figure 2.5: Position of the charges; $a = 320.6 \text{ mm}$, $m = 212.5 \text{ mm}$, $h = 550 \text{ mm}$.

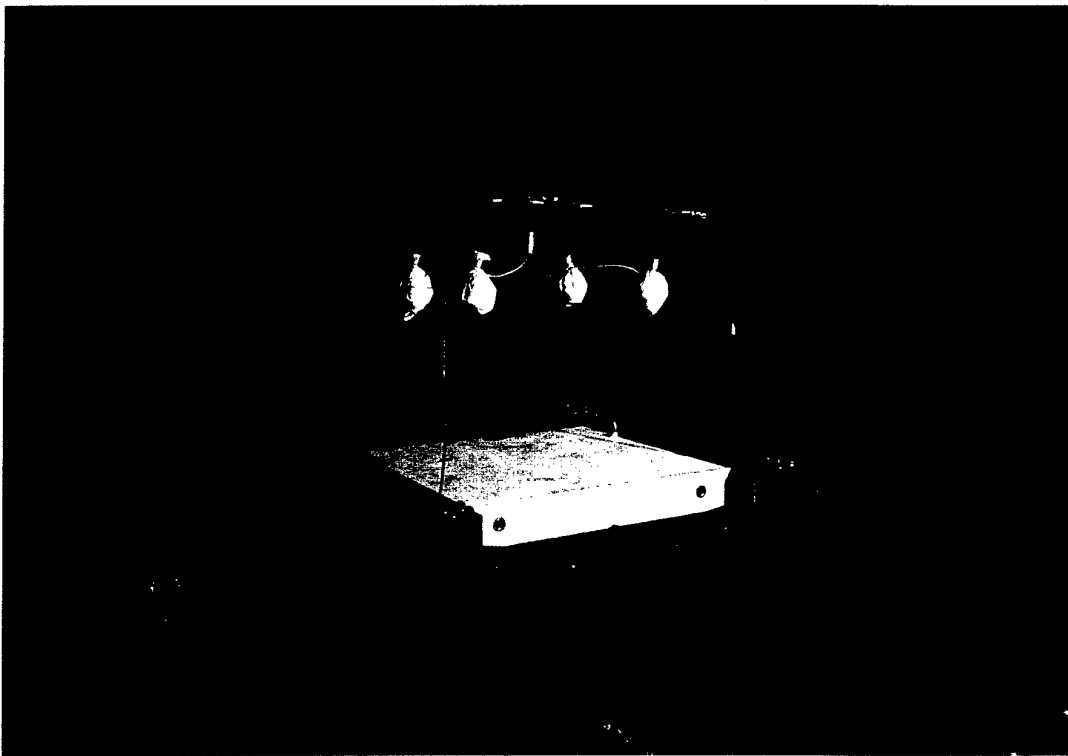


Figure 2.6: View of the complete test set-up with the charges.

2.4 Test programme

The slabs were supposed to fail in a single test. The necessary amount of explosive was estimated for each test. For safety of the measurement equipment, too high a charge was unwanted; the amount of explosive was chosen cautiously. This is the reason why it could happen that in some tests a slightly too small amount of ex-

plosive was used and that the slab did not fail. These slabs had to be loaded a second time.

An overview of the tests is given in Table 2.3. For the calculations and predictions, the reader is referred to Annex B.

Table 2.3: Overview of the tests.

Test no.	Slab no.	Amount of charge
1	7	4 x 0.85 kg
2	3	4 x 0.85 kg
3	3	4 x 0.75 kg
4	4	4 x 1.25 kg
5	6	4 x 0.75 kg
6	6	4 x 0.50 kg
7	1	4 x 1.25 kg
8	2	4 x 1.1 kg
9	5	4 x 0.85 kg
10	5	4 x 0.5 kg

2.5 Measurements

The measurements during the tests were principally the same as in the previous test series. Due to the different reinforcement and different test set-up, some displacement transducers and accelerometers had a slightly different position. The displacement was measured at four locations along the centre line of the slab. Contactless laser sensors, Micro-Epsilon model LD 1605, were used for these measurements. The acceleration was measured at three locations along the centre line of the slab. Four acceleration measurements were initially foreseen, but already in the first test, accelerometer A1 broke. ENDEVCO piezoresistive accelerometers, model 7270A were used here.

The measuring points for the load were different. Since we could not be certain of a uniformly distributed pressure, the load had to be measured at several locations on the slab. A compromise was made here between measuring the load correctly and not disturbing the response of the slab. Therefore, one pressure transducer was fixed in the slab; a second pressure transducer was placed next to the slab.

Since the shock wave could also enter the space underneath the reaction frame and thus load the back of the slab, a third pressure transducer was used to measure the pressure underneath the slab. All pressure transducers used were Druck Miniature Semiconductor Pressure Transducers, Type ENDEVCO model 8511A.

The positions of all measurements are given in Figure 2.7.

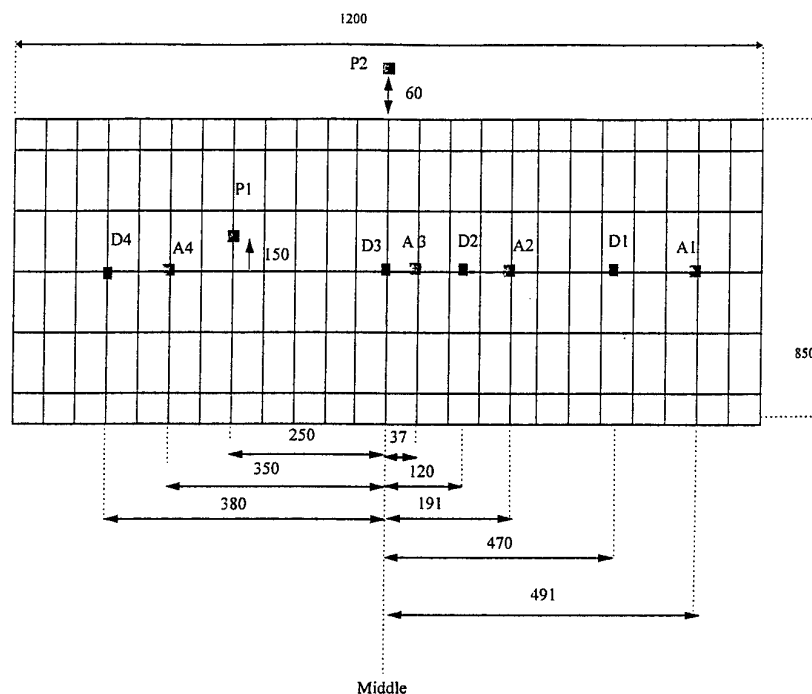


*Figure 2.7: Instrumentation of the slab, co-ordinates in mm
(A = acceleration, D = displacement and P = pressure).*

The protective measures for the equipment were similar to those in the previous test series. The laser transducers were surrounded by a steel frame, which would stop the concrete slab in its motion before it could hit the transducers. The position of this frame was such that the accelerometers on the slab would not hit the frame. Yet accelerometer A1 did break. This accelerometer was too close to the support and got stuck between the support and the slab.

3 Results

3.1 Introduction

In this chapter, the results of the tests are presented. The crack patterns of the slabs are given and the resistance-deformation curves, which are deduced from the measurements.

A remark is necessary about these resistance-deformation curves. The analysis method to derive these curves was supposed to be similar to that in the previous tests with the blast simulator. However, many problems were encountered. These problems are described here too.

A result for the resistance-deformation curve was found for the last part of the deformation process. From this curve the deformation capacity has been read. This value must however be used with care. As a consequence of the problems, the results may be liable for discussion.

3.2 Problems

Several problems were encountered.

- 1 The shock load on the slab, which was generated by detonating four charges simultaneously, is not uniformly distributed. Therefore, it is not possible to determine the total load on the slab correctly with one single measurement. Since the load is impulsive with respect to the response time of the slab, the impulse of the shock load is more important than the peak pressure. This impulse can be considered as approximately uniformly distributed. This quantity is far less sensitive to the location than the peak pressure. See Annex C for more information about the shock load.
- 2 The resistance of the slab is some orders lower than the peak load on the slab and the inertia forces of the slab. As a consequence, the resistance is of the same order as the noise over the measured load and acceleration. Therefore, it is very difficult to determine the maximum resistance of the slab and the point of failure.
- 3 The laser transducers, which were used for measuring the displacements, were disturbed too long by the flash of the explosion to find the deflection of the slab at failure. As a last resource, the acceleration signals were integrated twice in order to estimate the deformation as a function of time.
- 4 In the response, the third mode of the slab was clearly present. Although it damps out before the slab fails, it could not be neglected, and had to be taken into account in the analysis. The presence of this third mode is due to the impulsive character of the load. This effect is enhanced by the positions of the charges with respect to the slab.

3.3 Approach for determining the resistance-deformation curve

The resistance was determined according to the equation of motion. It is mathematically given by:

$$R(t) = F(P1) - F(P3) - M_{eff} \cdot a(t) \quad (3.1)$$

$F(P1)$ is the load on the slab according to the pressure measurement at location $P1$. During the shock load, this measurement is not representative of the pressure at other locations, but after the first shock has gone, it is. The quasi-static pressure which follows after the first shock load due to gas pressure can be considered as uniformly distributed.

$F(P3)$ is the load underneath the slab. Because the frame is open at the sides, the shock load can enter the space underneath the slab and cause a counterpressure for the motion of the slab.

$M_{eff}a(t)$ is the inertia force of the whole slab. For this inertia force, only the first mode has been taken into account, although initially the third mode is clearly present. Thanks to orthogonality (see [7]) each mode can be considered separately. Furthermore, during the analysis, it was observed that the third mode damps out without any remaining deformation. So, this mode does not contribute to the final failure of the slab.

The deformation is found from the acceleration measurements by integrating it twice. It appeared that the plastic deformation shape could not be represented by a single hinge in the centre as is done theoretically in the single degree of freedom method. A large plastic zone was observed on the slab. This means that the plastic deformation shape resembles the elastic deformation shape and that they cannot be separated from each other (see Annex D).

The accelerations and displacements are split up into the contributions of the first mode and the third mode as follows:

$$d(x) = \phi_{m1}(x) \cdot d_{m1}(0) + \phi_{m3}(x) \cdot d_{m3}(0) \quad (3.2)$$

and

$$a(x) = \phi_{m1}(x) \cdot a_{m1}(0) + \phi_{m3}(x) \cdot a_{m3}(0) \quad (3.3)$$

This gives a set of respectively four and three equations with two unknowns, which can be solved with the method of least squares. See Annex D for the set of equations.

The deformation for the first mode (obtained by integrating the acceleration twice) can now be related to the resistance to find the resistance-deformation curve. This curve is only used to estimate the ultimate deformation; it is not possible to determine other parameters from it.

3.4 Test 1 - Slab 7

Test 1 on slab 7 was performed on April 17th, 1997. The slab was loaded by four separate charges of 0.85 kg. This loading brought the slab to failure. The crack pattern is sketched in Figure 3.1. Figure 3.2 shows the damaged slab. The slab failed at location $x = -50$ mm. The position and size of the different cracks are listed in Table 3.1. The cracks which are not mentioned are hair cracks.

Table 3.1: Crack pattern of slab 7 in test 1.

crack number	1	2	3	4	5	6	7	8	9
size [mm]	2.5	1	0.8	24	26	12	1.5	4.8	0.5
position [mm]	-250	-200	-150	-100	-50	0	50	100	200

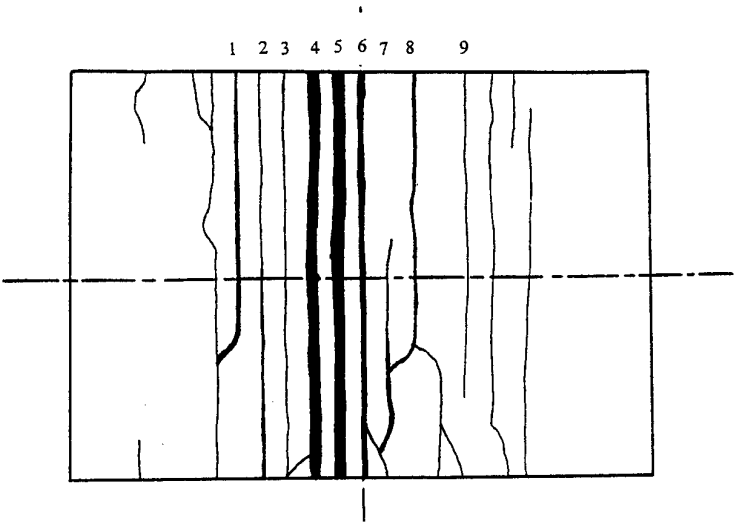


Figure 3.1: Global crack pattern of slab 7 after test 1.

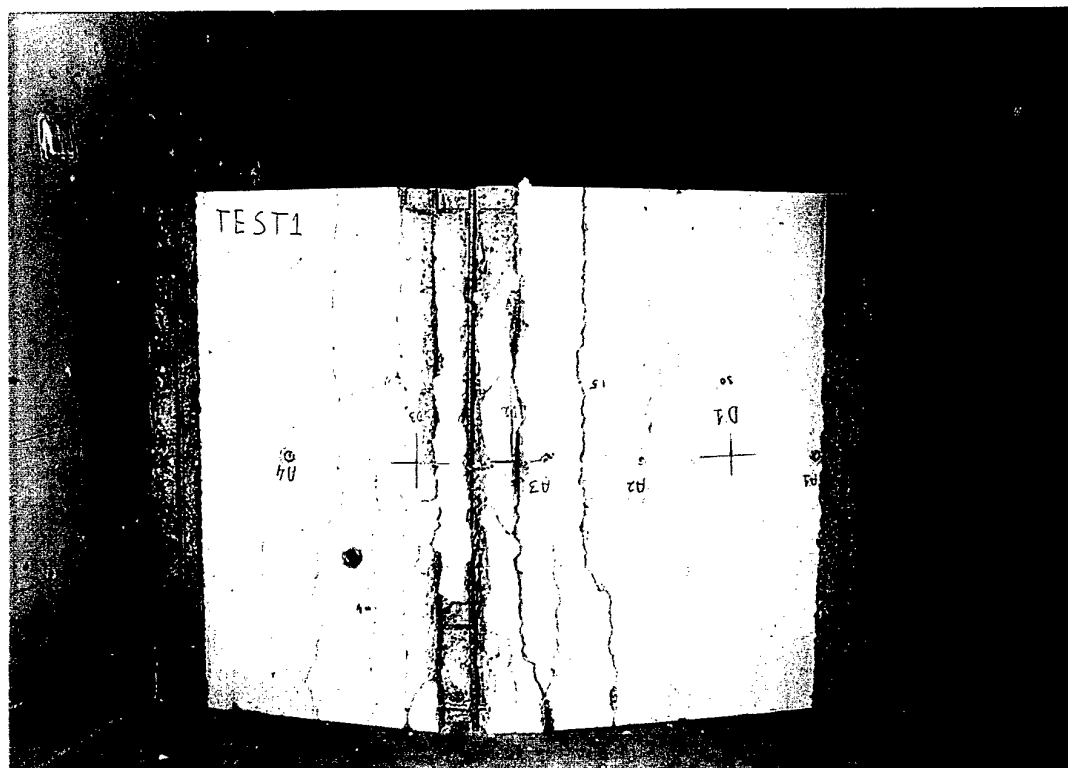


Figure 3.2: Slab 7 after test 1.

In this test, P_3 was not measured, because the reaction frame was closed on all sides. Since the shock wave could thus enter the space underneath the slab only through the small slits next to the slab, it was thought negligible. However, after the test, the plates closing the openings in the reaction frame appeared to be pushed outwards. Apparently a pressure had built up underneath the slab. This counter-pressure is probably not negligible. Even so we tried to calculate the resistance neglecting P_3 . The result is given in Figure 3.3.

From this curve, the point in time $t \approx 8.5$ ms seems to be the moment of failure. The indicators for this point in time are only weak. A decrease in the order of 200 kN in the resistance can be seen, which is the order of the ultimate resistance (see Annex B). And from this point in time, the resistance is around zero. Furthermore, the higher frequency of the noise at this point in time indicates a change in behaviour of the slab.

The resistance-deformation curve is given in Figure 3.4. From this curve, it can be seen that the ultimate deformation is approximately 51 mm. This deformation corresponds to a support rotation of 5.3° .

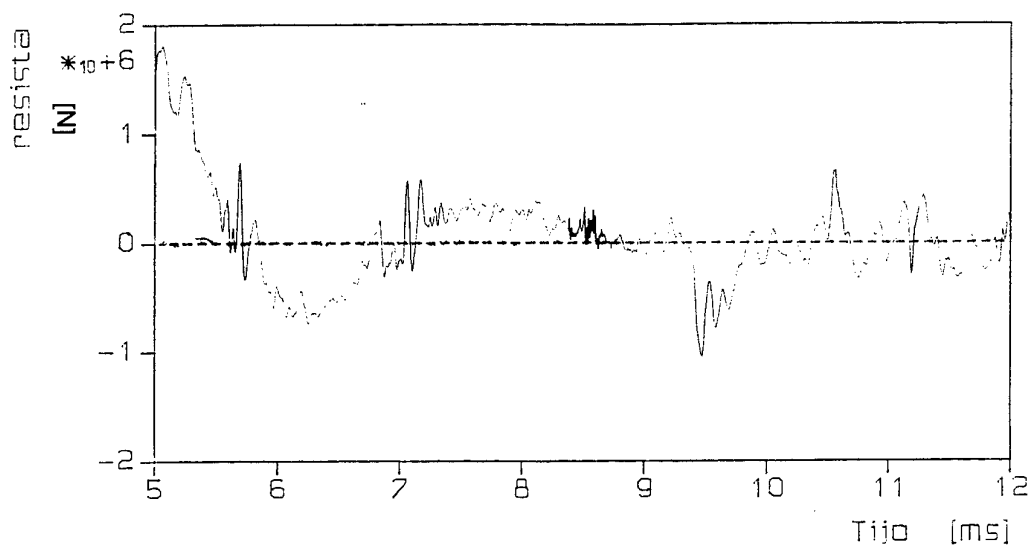


Figure 3.3: Calculated resistance of slab 7.

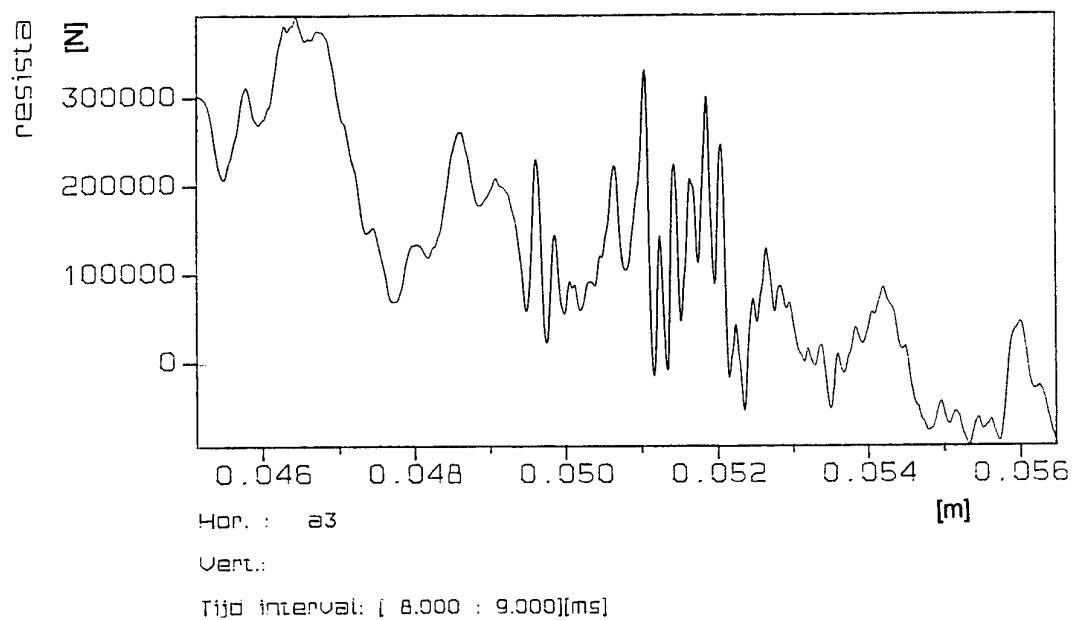


Figure 3.4: Resistance-deformation curve of slab 7.

3.5 Tests 2 and 3 - Slab 3

Test 2 was performed on April 18th, 1997. Slab 3 was loaded by four separate charges of 0.85 kg. During the test, the panels in front of the openings in the reac-

tion frame were left in their deformed shape, thus covering the openings only partly. The loading was insufficient to bring the slab to failure. The maximum deformation of the slab was located exactly in the centre. It was measured to be 59 mm.

Test 3 was performed on April 21st, 1997. Slab 3 was loaded again by four separate charges of 0.75 kg. The panels closing the sides of the reaction frame were removed and a pressure transducer was installed on the frame (location P3) to measure the overpressure under the slab. This new measured signal has been used for all the other tests.

During the test, the slab was brought to failure. The crack pattern is sketched in Figure 3.5. Figure 3.6 shows the damaged slab. The slab failed in the centre. The position and the size of the different cracks are listed in Table 3.2. Only macro cracks are considered.

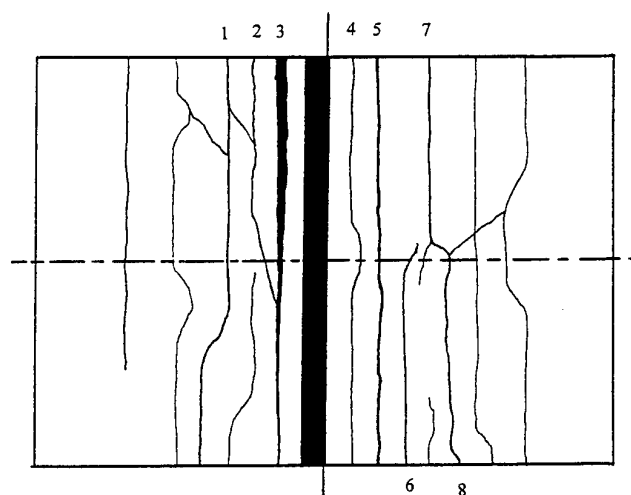


Figure 3.5: Global crack pattern of slab 3 after test 3.

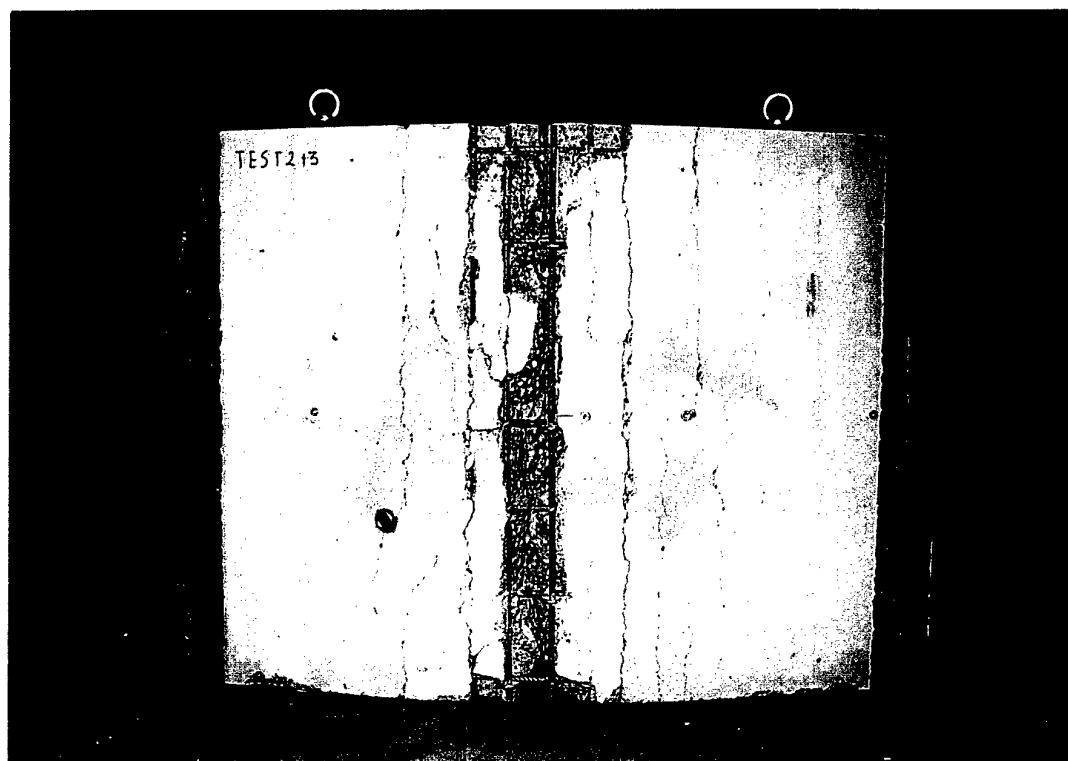


Figure 3.6: Slab 3 after test 3.

Table 3.2: Crack pattern in slab 3.

crack number	1	2	3	4	5	6	7	8
size [mm]	1	1.2	21	1	1.5	1	1	1
position [mm]	-200	-150	-100	50	100	150	200	250

It can be noticed that the concrete has completely spalled in the area between $x = -50$ mm and $x = 0$ mm.

We tried to determine the resistance of the slab. The result is given in Figure 3.7. From this curve, it is difficult to read the moment of failure. The resistance is already around zero when the disturbances in the signal diminish. It might be that the slab already failed in the beginning. But observing the higher frequency from time $t \approx 6.6$ ms, this point in time might also be the moment of failure.

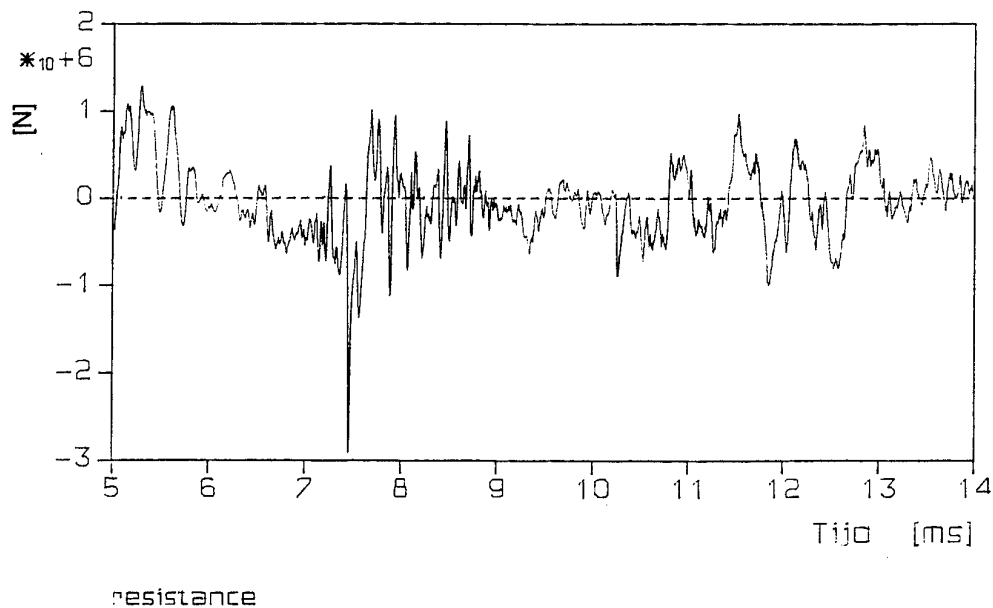


Figure 3.7: Resistance of slab 3 in test 3.

The resistance-deformation curve of this test is plotted in Figure 3.8. The deformation in this curve is a Δd . That means that this deformation should be added to the permanent deformation after test 2 to find the total deformation of the slab. From the resistance-deformation curve, it can be read that Δd is maximally 29 mm. For the maximum deformation capacity of slab 3, it can be concluded that it lies between 59 mm and 88 mm, which corresponds to support rotations of respectively 6.1° and 9.1° .

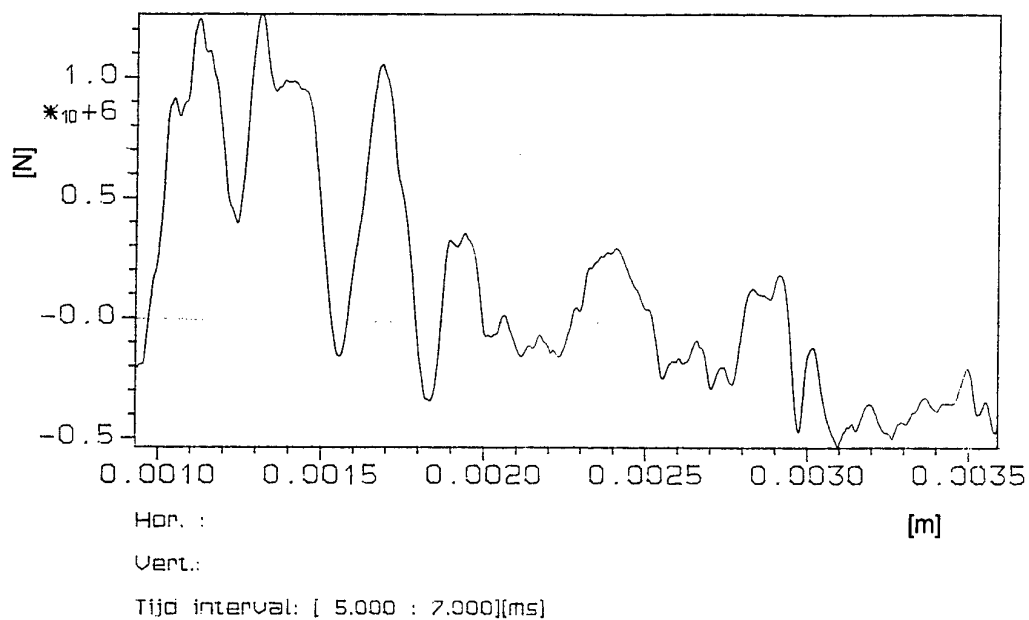


Figure 3.8: Resistance-deformation curve of slab 3 in test 3.

3.6 Test 4 - slab 4

This test was performed on April 22nd, 1997. Slab 4 was loaded by four separate charges of 1.25 kg. The slab failed during the test. The crack pattern is sketched in Figure 3.9. Figure 3.10 shows the damaged slab.

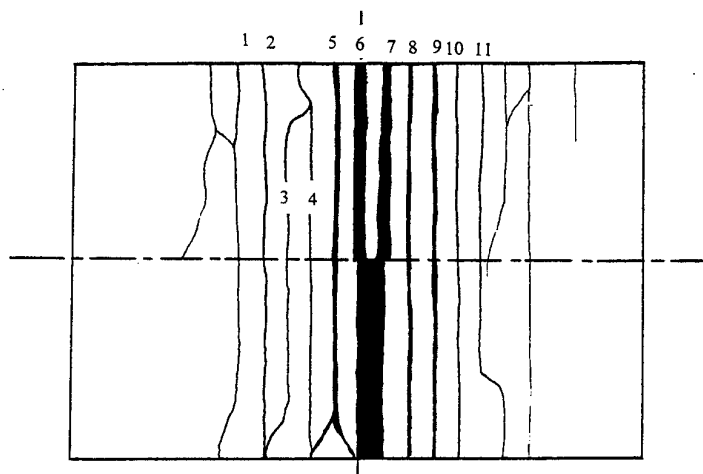


Figure 3.9: Global crack pattern in slab 4 after test 4.

The slab failed at location $x = 50$ mm. The position and the size of the different cracks are listed in Table 3.3. The cracks which are not mentioned are hair cracks.

Table 3.3: Crack pattern in slab 4.

crack number	1	2	3	4	5	6	7	8	9	10	11
size [mm]	1	2.3	1.1	2	5	25	26	4	3	1.5	1.2
position [mm]	-250	-200	-150	-100	-50	0	50	100	150	200	250

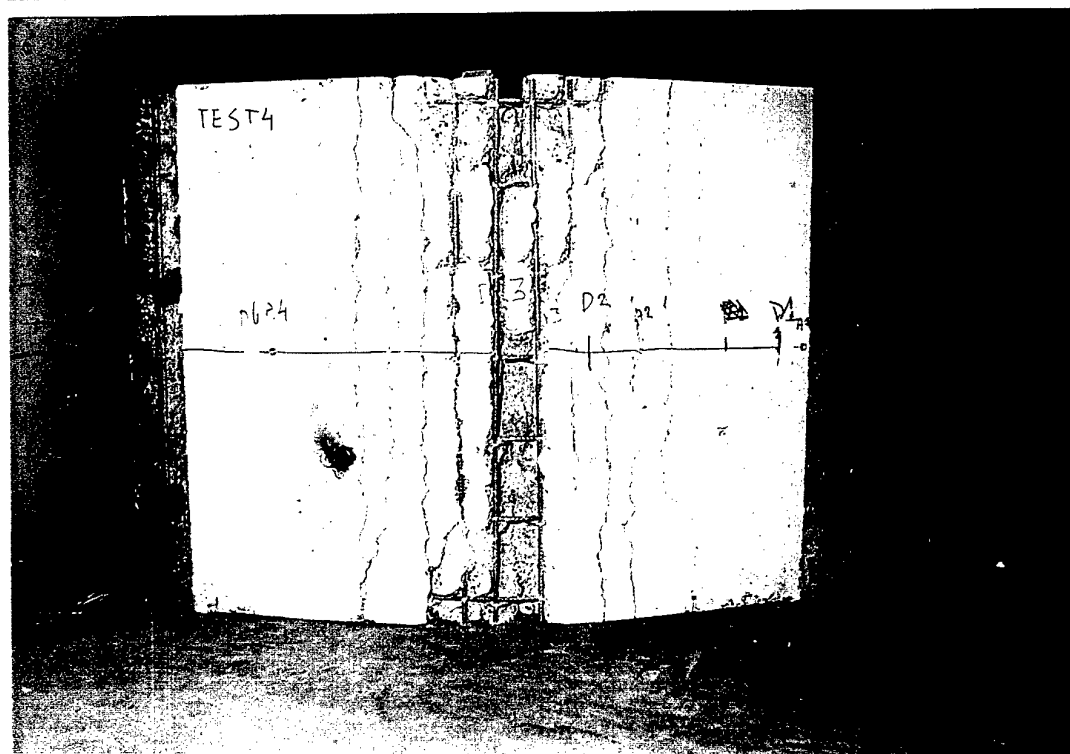


Figure 3.10: Slab 4 after test 4.

The resistance as a function of time is given in Figure 3.11. From this curve, $t \approx 9$ ms is estimated to be the moment of failure. A decrease in resistance in the order of 200 kN is seen and from this point in time on, the resistance is around zero. With the use of the resistance-deformation curve, which is given in Figure 3.12, an estimation of the ultimate deformation can be found. A value of 91.6 mm is read for this parameter. This corresponds to a support rotation of 9.5° .

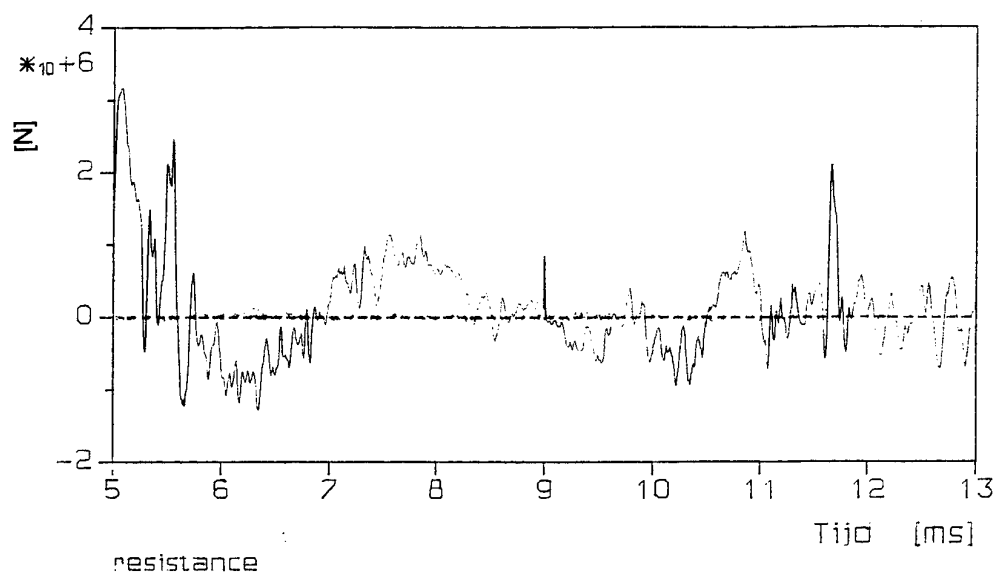


Figure 3.11: Resistance of slab 4 in test 4.

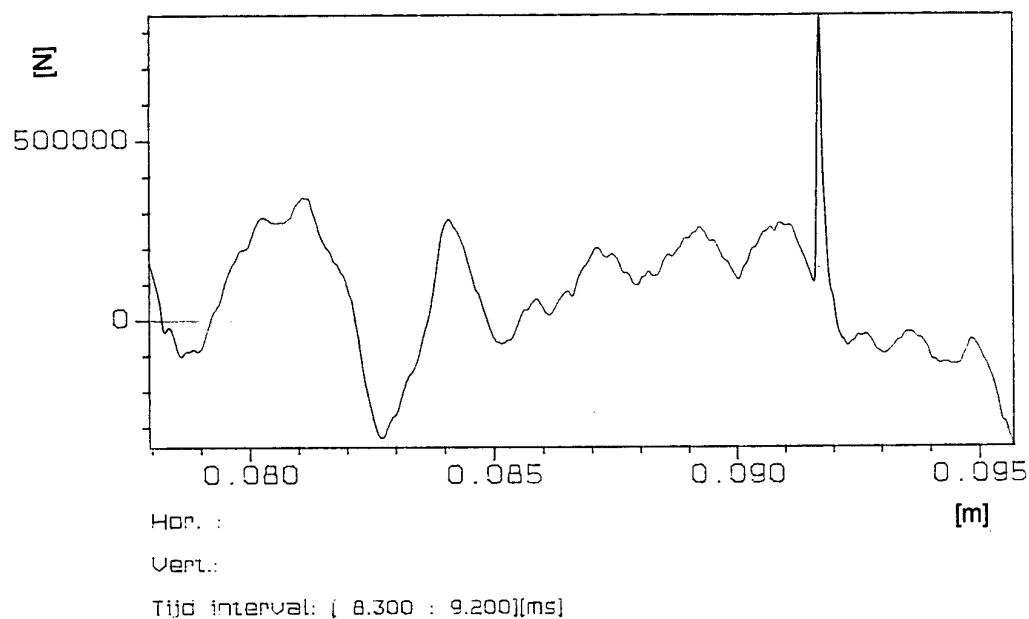


Figure 3.12: Resistance-deformation curve of slab 4 in test 4.

3.7 Test 5+6 - Slab 6

Test 5 was performed on April 22nd, 1997. Slab 6 was loaded by four separate charges of 0.75 kg. This loading did not bring the slab to failure. The maximum deformation of the slab was located in the centre. This was equal to 55 mm. Test 6 was performed on April 23rd, 1997. Slab 6 was loaded again by four separate charges of 0.5 kg. During the test, the slab was brought to failure. The crack pattern is sketched in Figure 3.13. Figure 3.14 shows the damaged slab.

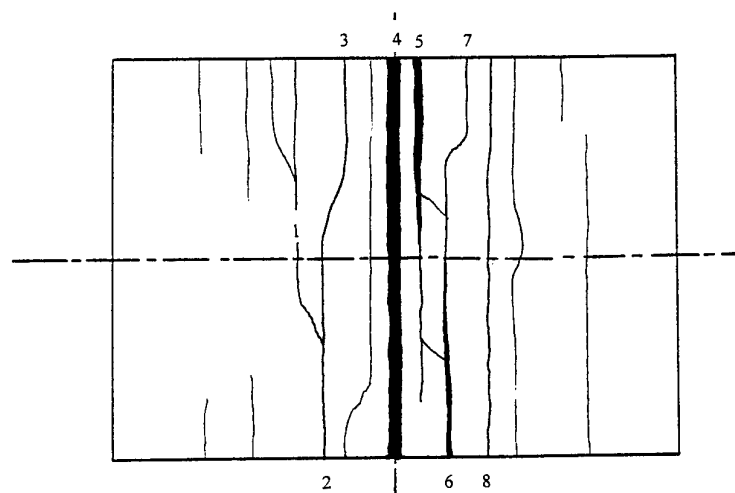


Figure 3.13: Global crack pattern in slab 6 after test 6.

The slab failed in the centre. The position and the size of the different cracks are listed in Table 3.4. The cracks which are not mentioned are hair cracks.

Table 3.4: Crack pattern in slab 6.

crack number	1	2	3	4	5	6	7	8
size [mm]	1	2.2	2	41.6	22.4	15	1.7	2.3
position [mm]	-200	-150	-100	0	50	100	150	200

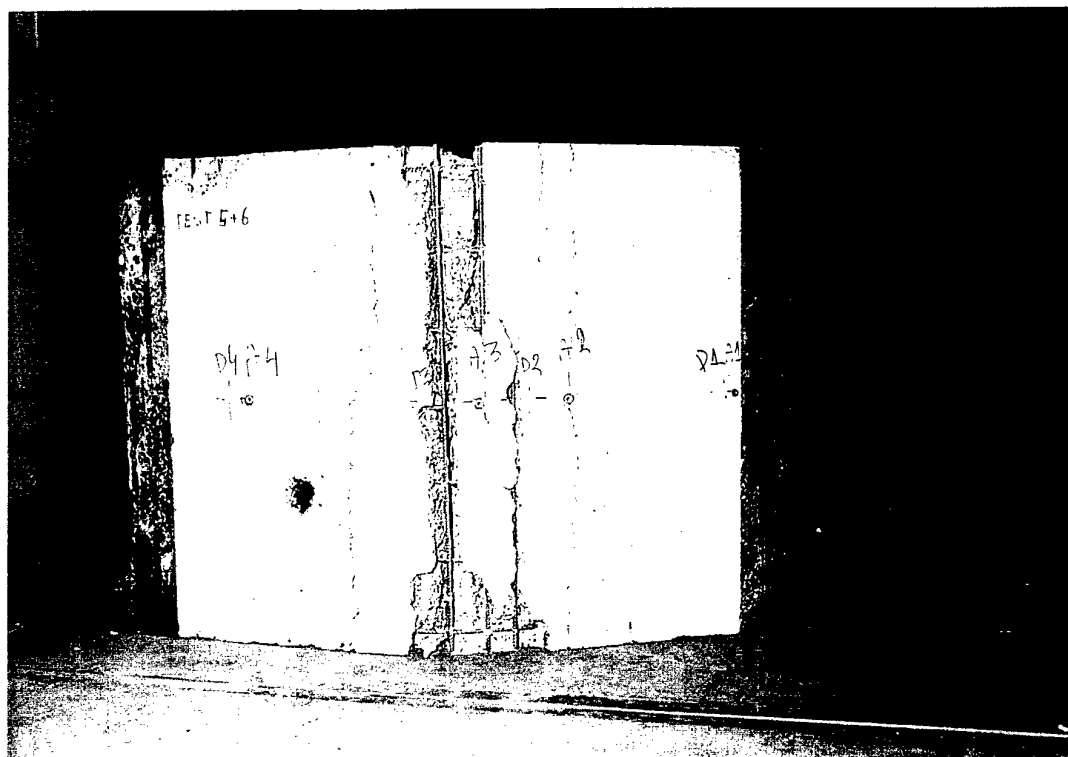


Figure 3.14: Slab 6 after test 6.

The resistance as a function of time is given in Figure 3.15. From this curve, $t \approx 6.6$ ms is estimated to be the moment of failure. A decrease in resistance in the order of 200 kN is seen and from this point in time on, the resistance is around zero.

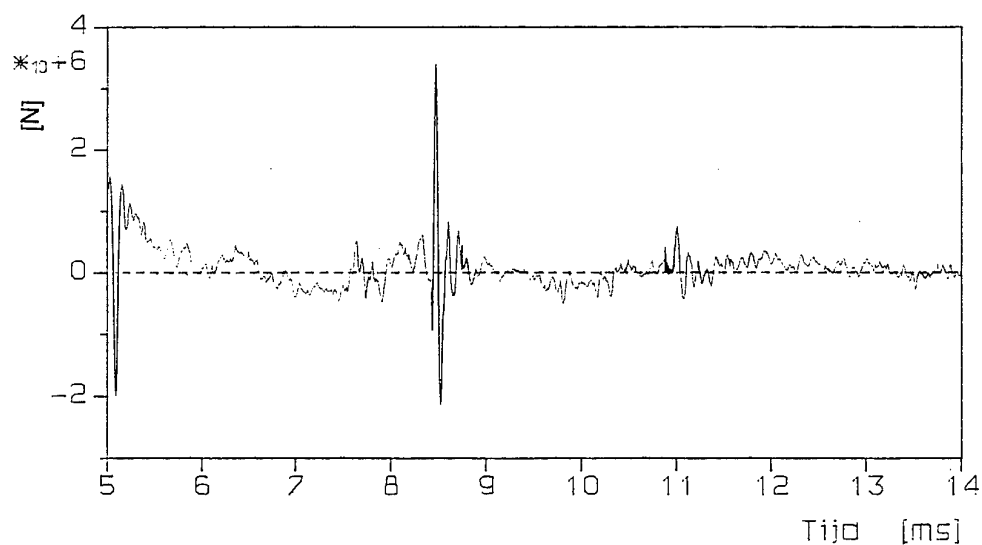


Figure 3.15: Resistance of slab 6 in test 6.

The resistance-deformation curve in Figure 3.16 gives the resistance as a function of the change in deformation Δd . The slab seems to undergo an extra deformation of 21 mm before it fails. The ultimate deformation of the slab lies then between 50 mm and 71 mm, or 5.2° and 7.4° .

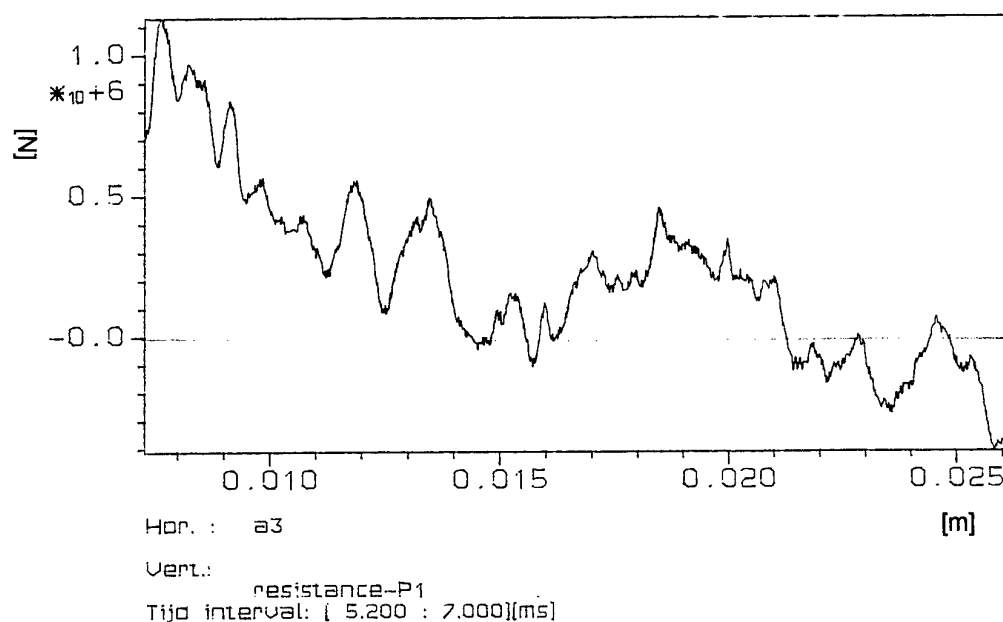


Figure 3.16: Resistance-deformation curve of slab 6 in test 6.

3.8 Test 7 - Slab 1

This test was performed on April 24th, 1997. Slab 1 was loaded by four separate charges of 1.25 kg. The slab failed during the test. The crack pattern is sketched in Figure 3.17. Figure 3.18 shows the damaged slab.

The slab failed at location $x = 50$ mm. The position and the size of the different cracks are listed in Table 3.5. The cracks which are not mentioned are hair cracks.

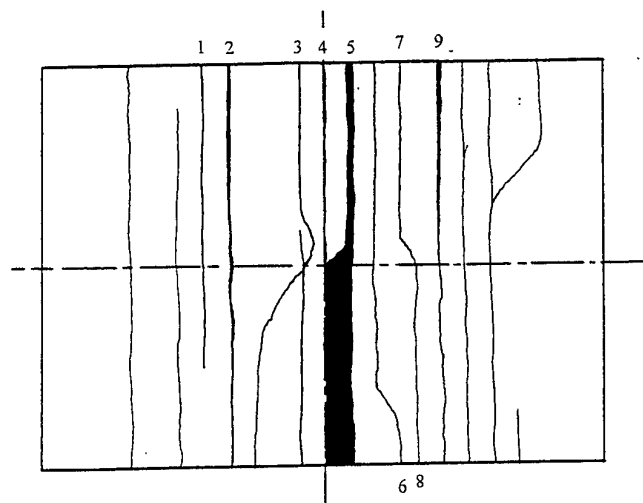


Figure 3.17: Global crack pattern in slab 1.

Table 3.5: Crack pattern in slab 1.

crack number	1	2	3	4	5	6	7	8	9
size [mm]	0.8	1.4	1.8	2.3	31	1.2	1.3	1.3	1.3
position [mm]	-250	-200	-50	0	50	150	150	200	250

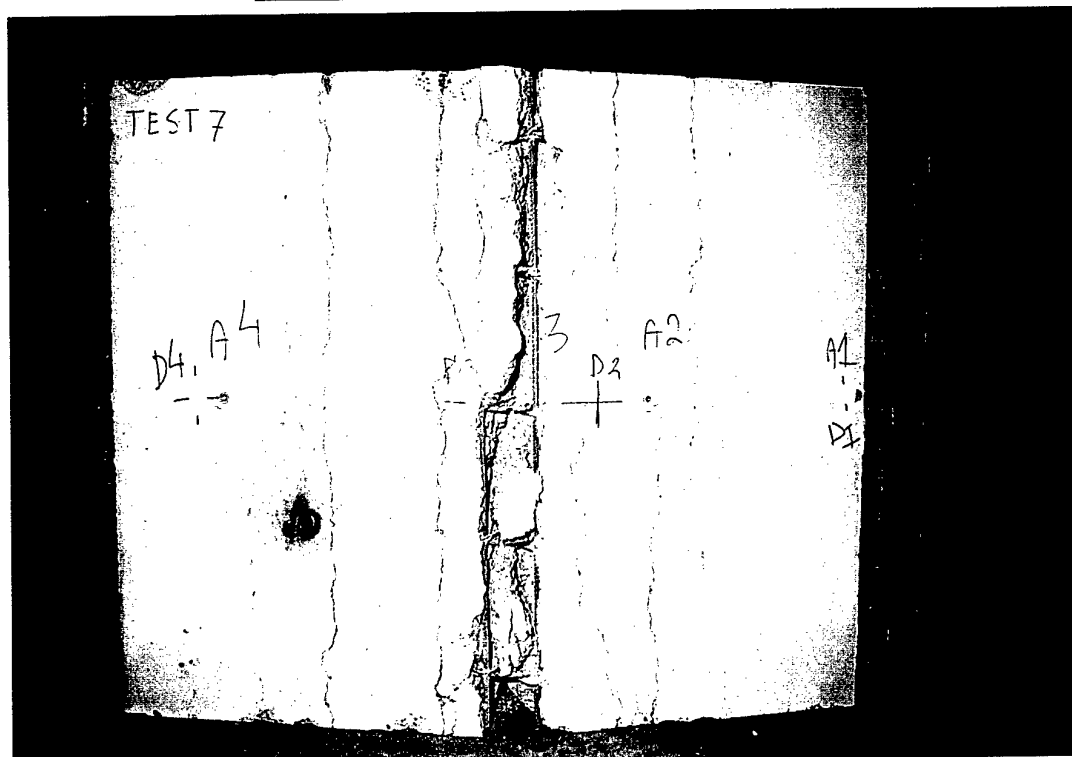


Figure 3.18: Slab 1 after test 7.

The resistance as a function of time is given in Figure 3.19. From this curve, $t \approx 10.6$ ms is estimated to be the moment of failure. A decrease in resistance in the order of 200 kN is seen and from this point in time on, the resistance is around zero. Furthermore, the high peaks in the resistance at this point in time, indicate a change in behaviour.

From the resistance-deformation curve, given in Figure 3.20, an ultimate deformation of 102 mm can be read. This deformation corresponds to a support rotation of 10.5° .

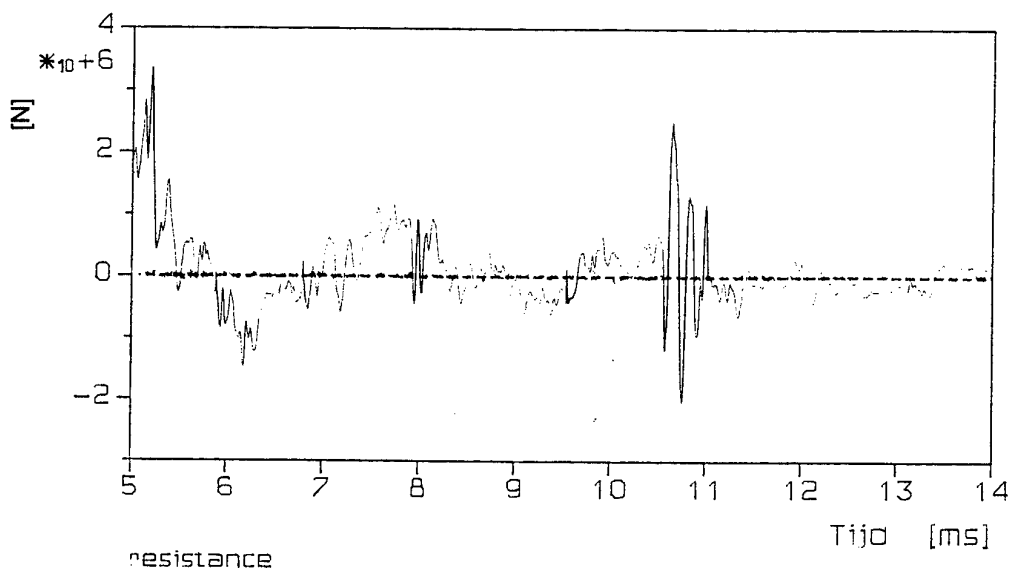


Figure 3.19: Resistance of slab 1 in test 7.

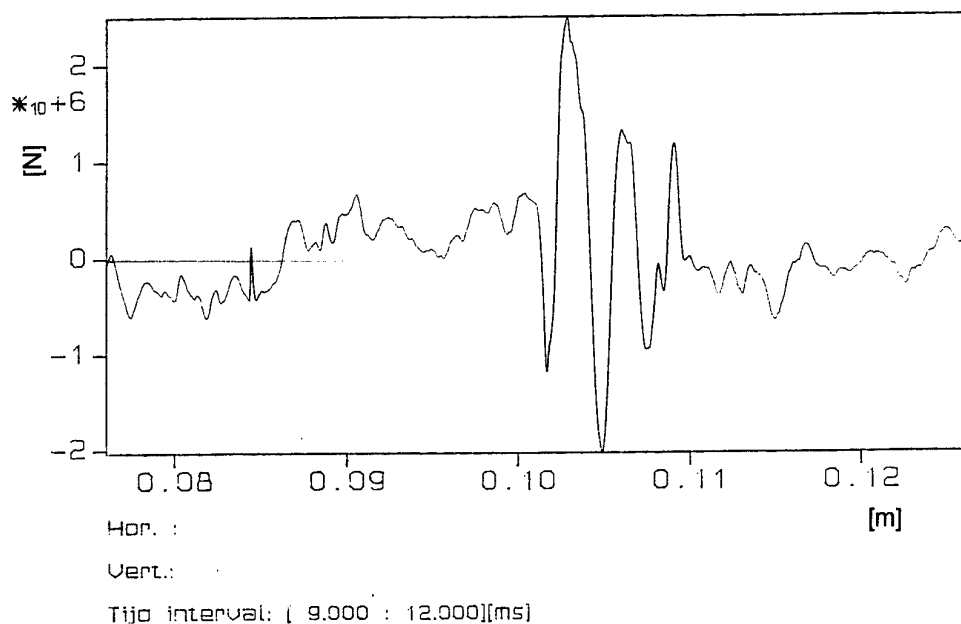


Figure 3.20: Resistance-deformation curve of slab 1 in test 7.

3.9 Test 8 - Slab 2

This test was performed on April 25th, 1997. Slab 2 was loaded by four separate charges of 1.1 kg. This loading was sufficient to bring the slab to failure. The crack pattern is sketched in Figure 3.21. Figure 3.22 shows the damaged slab.

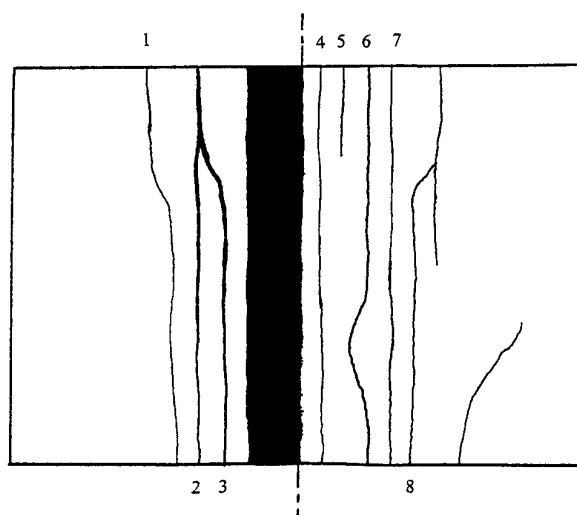


Figure 3.21: Global crack pattern in slab 2 after test 8.

The slab failed at location $x = -50$ mm. The position and the size of the different cracks are listed in Table 3.6. The cracks which are not mentioned are hair cracks.

Table 3.6: Crack pattern in slab 2.

crack number	1	2	3	4	5	6	7	8
size [mm]	0.8	0.8	12	1	0.8	1.9	0.7	1.4
position [mm]	-300	-200	-150	50	100	150	200	250

The concrete in the area between $x = -100$ mm and $x = 0$ mm has completely spalled.

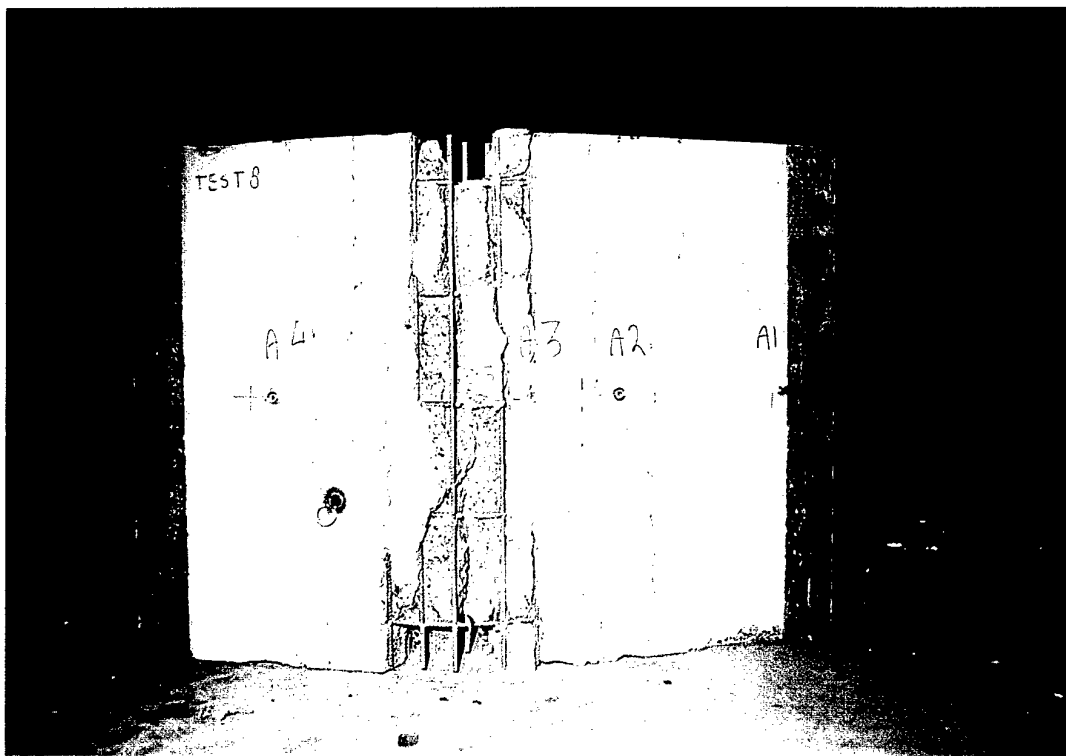


Figure 3.22: Slab 2 after test 8.

The resistance of slab 2 as a function of time is given in Figure 3.23. A decrease in the resistance of the order of 200 kN can be observed at time $t \approx 14$ ms, and after this decrease, the resistance remains around zero. Shortly after this point in time, there are also high disturbances in the signal.

The resistance-deformation curve is given in Figure 3.24. From this curve the ultimate deformation of slab 2 is read to be approximately 103 mm. This deformation corresponds to a support rotation of 10.6° .

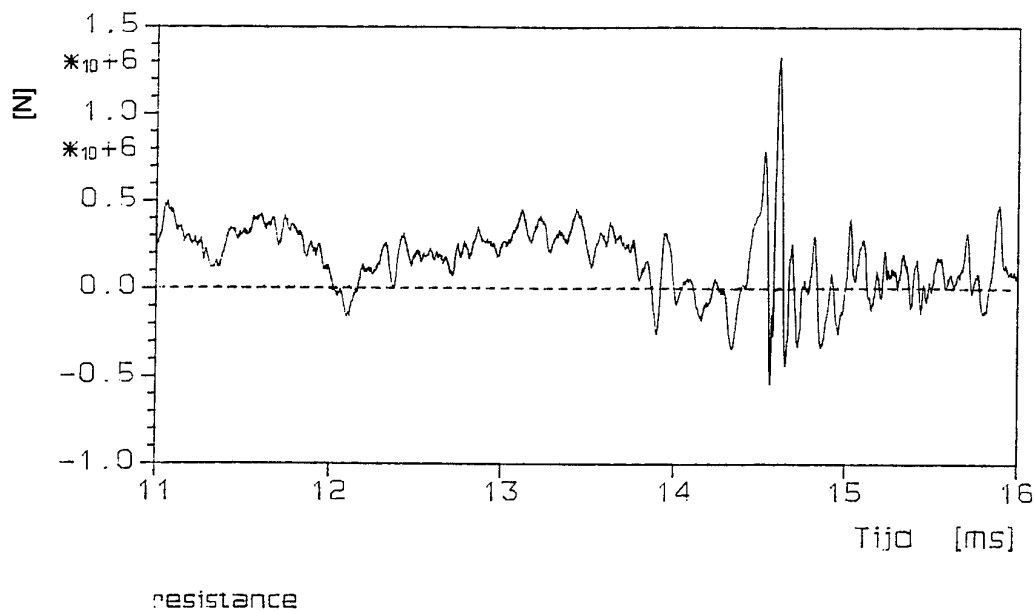


Figure 3.23: Resistance of slab 2 in test 8.

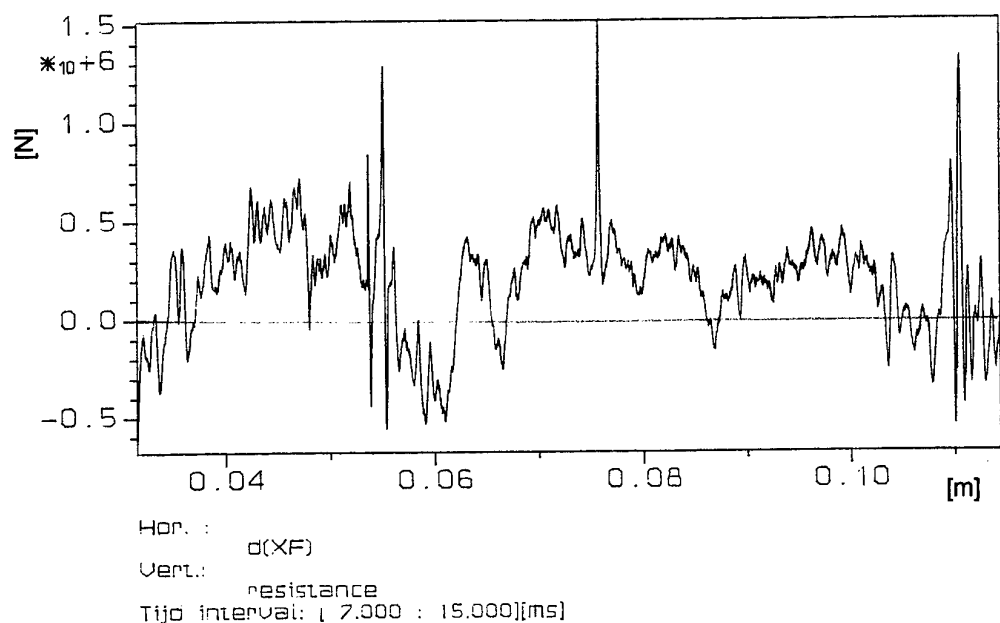


Figure 3.24: Resistance-deformation curve of slab 2 in test 8.

3.10 Test 9+10 - Slab 5

Test 9 was performed on April 28th, 1997. Slab 5 was loaded by four separate charges of 0.85 kg. The loading was not sufficient to bring the slab to failure. The permanent deflection in the centre was equal to 60 mm.

Test 10 was performed on April 28th, 1997. Slab 5 was loaded again, by four separate charges of 0.5 kg. This brought the slab to failure. The crack pattern is sketched in Figure 3.25. Figure 3.26 shows the damaged slab.

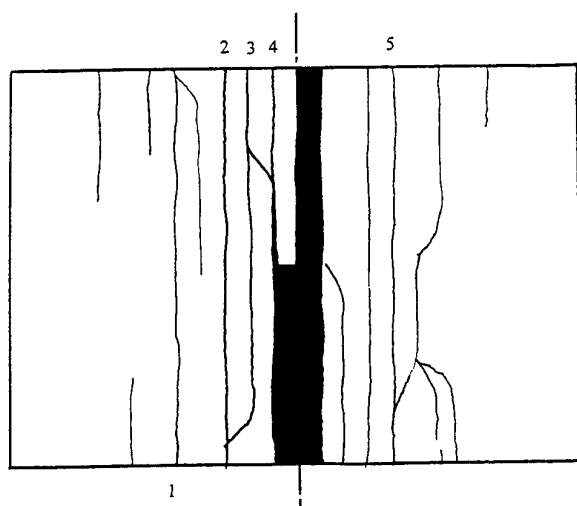


Figure 3.25: Global crack pattern in slab 5 after test 10.

The slab failed where the main deformation was located in test 9, that is at location $x = 25$ mm. The position and the size of the different cracks are listed in Table 3.7. The cracks which are not mentioned are hair cracks.

Table 3.7: Crack pattern in slab 5.

crack number	1	2	3	4	5
size [mm]	0.5	1.2	1.4	1.2	0.7
position [mm]	-250	-150	-100	-50	200

The concrete was completely crushed in the area between $x = -50$ mm and $x = 50$ mm.

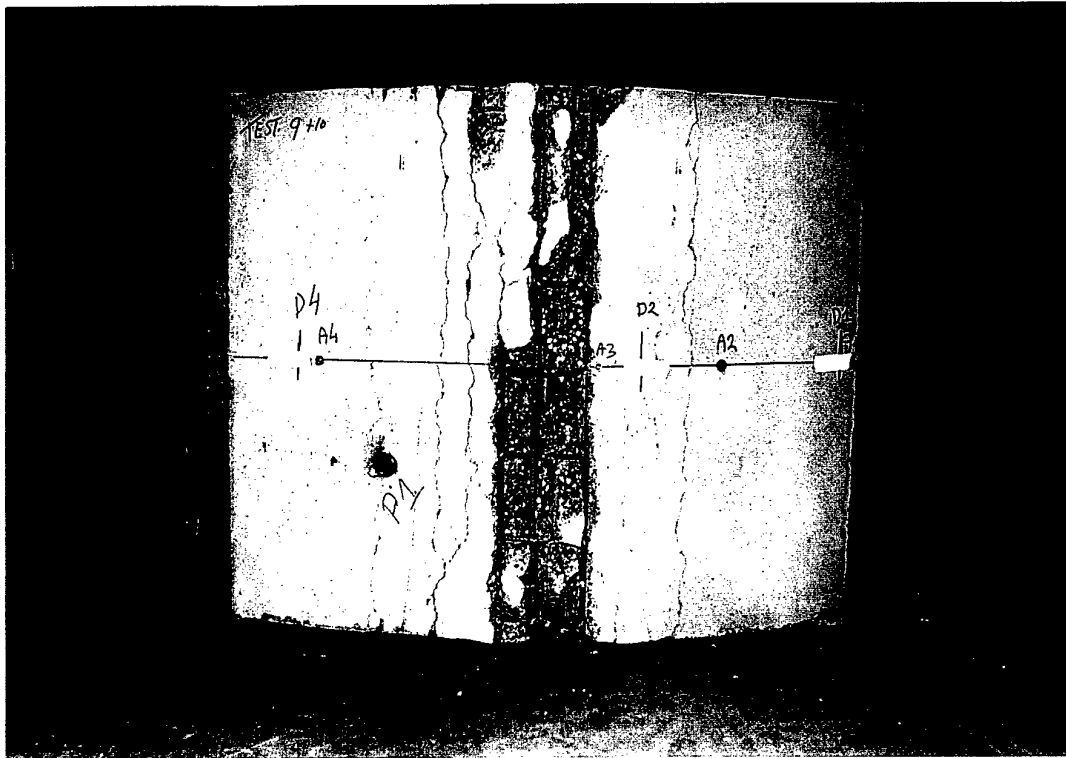


Figure 3.26: Slab 5 after test 10.

The resistance as a function of time is given in Figure 3.27. From this curve, time $t \approx 5.6$ ms can be pointed out as a possible point of failure.

The resistance-deformation curve in Figure 3.28 gives the resistance as a function of the change in deformation Δd . The slab seems to undergo an extra deformation of maximally 8 mm before it fails. The ultimate deformation of the slab lies then between 60 mm and 68 mm, or 6.2° and 7.0° .

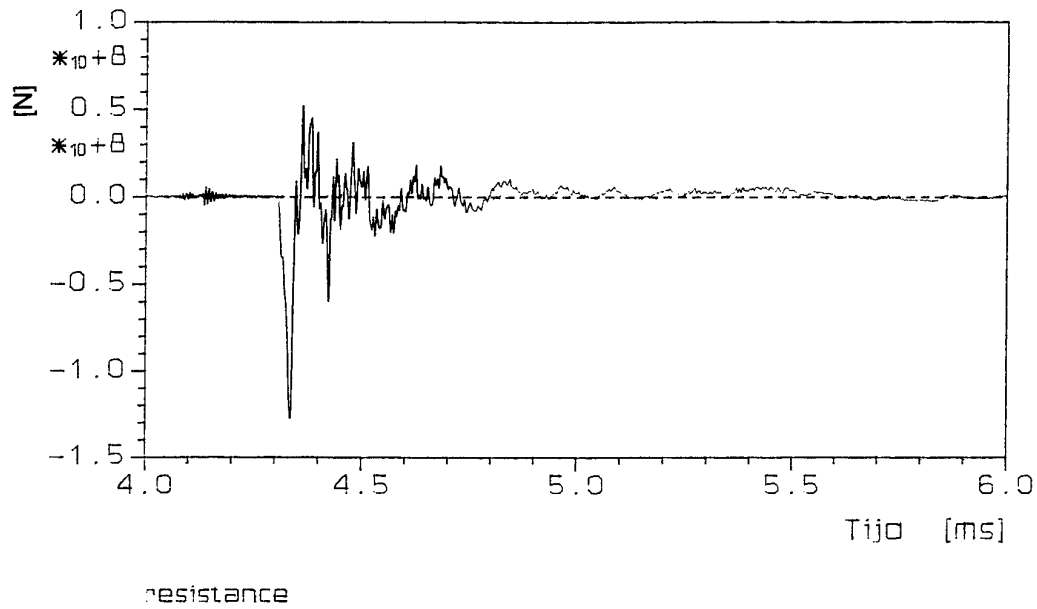


Figure 3.27: Resistance of slab 5 in test 10.

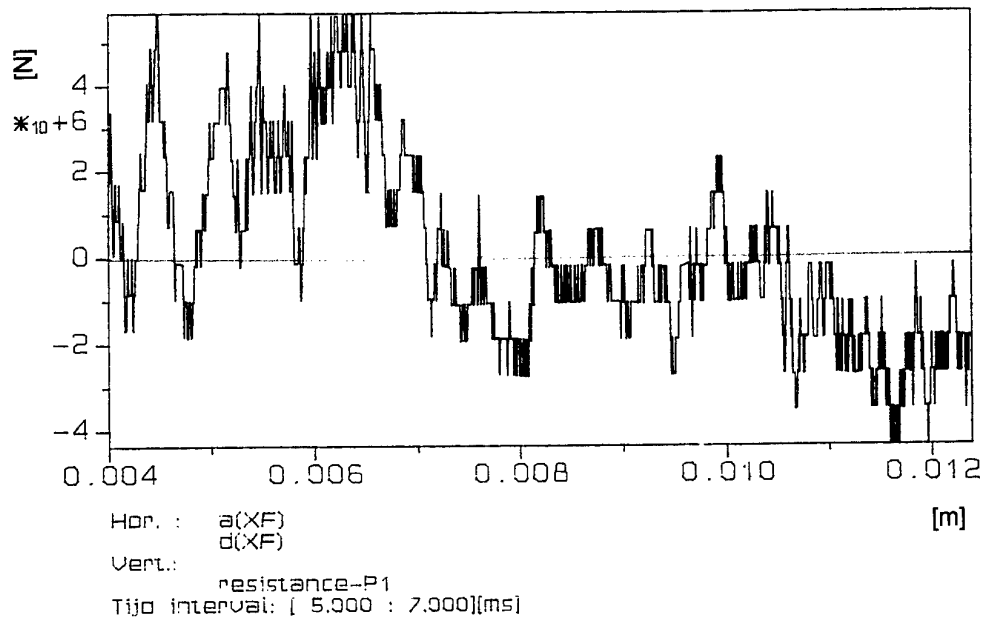


Figure 3.28: Resistance-deformation curve of slab 5 in test 10.

4 Discussion of results

4.1 Introduction

In the previous chapter, the results of the tests are presented. These results will be discussed in this chapter by comparing them with each other, with calculations according to TM 5-1300 and with the results of the previous test series.

4.2 Comparison of the present tests

To make the comparison easy, the results are summarised in Table 4.1. These results should be used with care, because of the reported difficulties in the analysis of the tests.

Table 4.1: Summary of test results.

Type of the slab		Ultimate deformation X_u (mm)	Support angle θ_u (degree)
Slabs without shear reinforcement			
Test 1	4.1.1	51	5.3
Tests (5+6)	4.1.1	$50 < X_u < 71$	$5.2 < \theta_u < 7.4$
Test 8	4.2.1	103	10.6
Tests (9+10)	4.1.1	$60 < X_u < 68$	$6.2 < \theta_u < 7.0$
Slabs with lacing			
Tests (2+3)	4.1.2	$59 < X_u < 88$	$6.1 < \theta_u < 9.1$
Test 4	4.1.2	91.6	9.5
Test 7	4.2.2	102	10.5

The following observations can be made.

- From the comparison of tests 1, (5+6) and (9+10), it can be concluded that the ultimate support rotation of the slabs of type 4.1.1 is in the order of 5.5° . For design purposes, the lower value is of prime importance because it determines the construction safety. So, the measured support rotation of 5.2° should be used as design criterion.
- The deformation capacity of the slabs of type 4.1.1, with the thin reinforcement, is lower than that of the slabs of type 4.2.1, with the thicker reinforcement steel. The longitudinal reinforcement with a diameter of 10 mm increased the maximum support rotation of the tested slabs by approximately 93% (from 5.5° to 10.6°) compared to the longitudinal reinforcement of 8 mm. It can be concluded that the diameter of the bending reinforcement has an important influence on the deformation capacity. Thick reinforcement rods have a favourable effect on the deformation capacity. As it is known from TM 5-1300 and previous results that buckling often initiates the failure of concrete slabs, the

reduced tendency of thick rods to buckle under a compressive load would explain the improvement in deformation capacity. This result confirms the results of the previous tests series [3].

- Slab type 4.1.2 has a much larger deformation capacity than slab type 4.1.1. The increase in deformation capacity is 70% (from 5.5° to 9.3°). Slab type 4.1.2 owes this larger deformation capacity to the thruss action of the lacing reinforcement; this prevents or delays the buckling failure.
- Slab types 4.2.1 and 4.2.2 have approximately the same deformation capacity. Apparently, the lacing in slab 4.2.2 is not effective to delay the failure of the slab. For this slab, the influence of the lacing is very small. The same ultimate deformation for both slab types and lacing seeming to be irrelevant might indicate that the failure mode has changed. Not the failure of the compression zone, but the failure of the tensile reinforcement might be the cause of structural failure. Then it is logical that lacing cannot increase the deformation capacity.

4.3 Comparison with TM 5-1300 calculations

Table 4.2 gives a comparison between the ultimate support rotation θ_u measured in the tests and the value prescribed by TM 5-1300.

Table 4.2: Comparison of test results with TM 5-1300.

Test	θ_u from test (°)	θ_u from TM 5-1300 (°)	slab type
1	5.3	2	4.1.1
2+3	$6.1 < \theta_u < 9.1$	12	4.1.2
4	9.5	12	4.1.2
5+6	$5.2 < \theta_u < 7.4$	2	4.1.1
7	10.5	12	4.2.2
8	10.6	2	4.2.1
9+10	$6.2 < \theta_u < 7.0$	2	4.1.1

The following observations can be made:

- the maximum deformation that is observed in the tests for the slabs without shear reinforcement is considerably higher than TM 5-1300 admits;
- for the slabs with lacing, that is for tests (2+3), 4 and 7, lower values are found for the ultimate support rotation than TM 5-1300 uses for design purposes. The results point out that TM 5-1300 should be used with care.

4.4 Comparison of the results with previous test results

As a result of the previous test programme, an empirical relationship was found, which states that the maximum support rotation of a simply supported reinforced

concrete slab without tying reinforcement can be described as a linear function of the following parameter:

$$X' = \phi^2/d$$

where:

ϕ = diameter of the longitudinal reinforcement;

d = effective depth of the slab.

The validity of this relationship is only proven for slabs which fit in the series of tested slabs. This is very limited. The limitations of the proven validity was given by:

- no shear reinforcement;
- support length = 1.1 m;
- 70 mm < thickness < 100 mm;
- 0.35% < reinforcement ratio < 0.64%;
- reinforcement steel: FeB500;
- 6 mm < diameter of longitudinal reinforcement < 8 mm;
- cube strength of concrete 40 to 50 MPa;
- the slabs fail in a single shock.

The slabs tested in this series do not satisfy the limitations of proven validity. Therefore, the results give us the opportunity to either extend the proven validity or demarcate the validity.

A summary of all the results is presented in Table 4.3.

Table 4.3: Summary of all test results.

Slab number	ϕ (mm)	d (mm)	X' (mm)	Measured deformation capacity (°)
1.1*	6	57	0.63	5.7
1.2*	6	57	0.63	5.8
2.1*	8	83	0.77	8
2.2*	6	82	0.44	2.5
3.1.1*	6	65	0.55	4.45
4.1.1	8	98	0.65	5.2-6.2
4.2.1	10	97	1.03	10.6

* indicates that the slabs belong to the previous test series.

The parameter X' and the maximum support rotation are plotted in Figure 4.1.

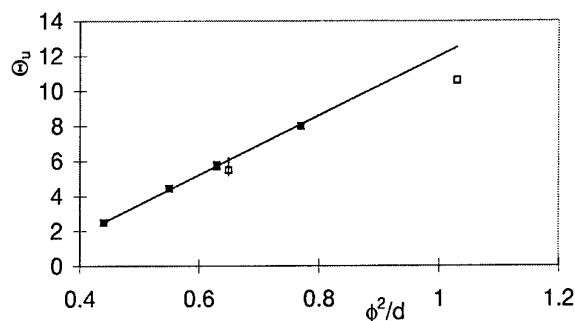


Figure 4.1: Maximum support rotation as a function of ϕ^2/d .

The ultimate deformation found for slab type 4.1.1 was a rough estimate. Taking the scatter in the results into account, it can be concluded that the result for this slab type fits the empirical relationship.

The value of the ultimate support rotation of slab type 4.2.1 does not fit the empirical relationship. For this slab, a change in failure mode was already surmised. Based on the observation that lacing does not increase the deformation capacity of this type of slab, a tensile failure was surmised which initiated complete failure, instead of crushing of the compression zone. With another failure mode, it is logical that the result does not fit in the empirical relation found in previous tests. This empirical relation gave a failure criterion in case compression failure is the criterion. For tensile failures, another criterion should be used. In the following section, we attempt to find such a criterion.

The types of slabs for which the validity of the empirical relationship in Figure 4.1 is proven can be extended to slabs with a thickness of 125 mm.

4.5 Criterion for tensile failure

From the stress distribution in the tensile steel, it follows that the deformation of the tensile steel is mainly limited to the positions of the cracks. Between the cracks, the steel stress will be below the yield stress, because part of the load is transferred to the concrete. The strains corresponding to a stress lower than the yield stress is small compared to the strains in the yielding parts of the steel, which is the debonded part of the steel in the cracks. Therefore, we will neglect the deformation in the parts between the cracks and concentrate on the deformation in the crack.

The rotation in a construction element can be found by integrating the curvature κ . That is given by:

$$\theta = \int \kappa dx \cong \int \frac{\epsilon}{T} dx = \sum_i \frac{\ell_i \epsilon_i}{T} \quad (4.1)$$

where ℓ_i is the length of debonded steel in crack i , and ε_i is the average strain in the steel in crack i and T is the thickness of the slab.

The debonded length ℓ is determined by the strains in the steel. Bonding is namely only possible when the concrete can follow the strain in the steel. So, debonding occurs as soon as the strain in the steel exceeds the cracking strain of the concrete. Suppose that σ_{bond} is the stress for the steel which corresponds with this strain. The force in the steel that must have been transferred to the concrete must be

$$F = \frac{1}{4} \pi \phi^2 (\sigma_{\text{yield}} - \sigma_{\text{bond}}) \quad (4.2)$$

The bond strength is given by τ_{bond} , and per unit length a force $\pi \phi \tau_{\text{bond}}$ can be transferred. Therefore, the debonded length satisfies the following equation:

$$\ell = \frac{(\sigma_{\text{yield}} - \sigma_{\text{bond}}) \pi \phi^2 / 4}{\pi \phi \tau_{\text{bond}}} \quad (4.3)$$

Combining equations (4.1) and (4.3) gives the result that the rotation in a crack is linearly proportional to $\phi \varepsilon_i / T$, using the fact that the same concrete and steel quality are used in all tests. That means the strength properties are the same for all slabs.

Since the same deformation shape can be assumed for all tested slabs, this result can be extended to the total deformation, the ultimate support rotation:

$$\theta_u \cong \frac{\phi}{T} \quad (4.4)$$

It is taken into account here that the limiting strain is the same for all tests, because the same steel quality is used.

The proportionality of the ultimate support rotation and the diameter of the longitudinal reinforcement has been checked for all the slabs with lacing. The result is plotted in Figure 4.2. The values used to draw the curve are presented in Table 4.4.

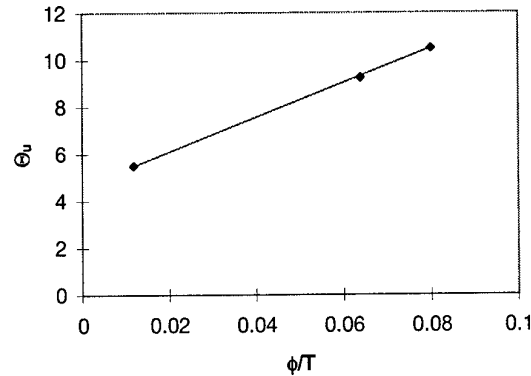


Figure 4.2: Empirical relationship for the deformation capacity of laced slabs.

Table 4.4: *Ultimate deformation capacity of laced slabs.*

Slab	ϕ (mm)	T (mm)	ϕ/T	θ (°)
4.2.2	10	125	0.080	10.5
4.1.2	8	125	0.064	9.5
3.3*	6	100	0.060	5.53

* the slab belongs to a former test series.

A new empirical relationship has been found for the ultimate support rotation of a simply supported slab, which fails due to failure of the tensile reinforcement. It does not necessarily have to be a slab with lacing, as is shown by test 8 on slab type 4.1.2.

The two empirical relationships should both be used to determine the ultimate deformation capacity of a reinforced concrete slab. The lower value gives the criterion for the slab in question.

The validity of this method with two empirical relationships is proven for slabs with the following characteristics:

- no shear reinforcement or lacing reinforcement;
- support length = 1.1 m;
- 70 mm < thickness < 125 mm;
- 0.35% < reinforcement ratio < 0.64%;
- reinforcement steel: FeB500;
- 6 mm < diameter of longitudinal reinforcement < 10 mm;
- cube strength of concrete 40 to 50 MPa;
- the slabs fail in a single shock.

With this result, the unexpected result in the previous test programme for the slabs with lacing (type 3.3) has been explained. This result fits in the empirical relationship. Tensile failure occurs far sooner than at 12 degrees support rotation as TM 5-1300 prescribes.

4.6 Discussion of the test method

Many difficulties were encountered in analysing the measurements. Before any further tests, the test method should therefore be analysed and modified.

- The displacement measurements were disturbed undesirably long by the flash of the explosion. The duration of the disturbance was shorter in test 1 than in the other tests. This was due to the fact that the reaction frame was closed. The laser transducers were shielded better from the flash. It should be possible to diminish the disturbance by shielding the laser transducers. If this appears to be insufficient, then other displacement transducers should be considered, which are not sensitive to light flashes.

- The applied pressure on the slab was not uniform. In this test series, it was concluded that this was not of major importance, because the loading is in the impulsive regime. If, however, a uniform pressure is required for other tests, then the only solution would be either to position the charge(s) at a further distance or to use a plate of explosive, which has to be initiated at several locations. Several pressure transducers should be used to check the uniformity of the load.
- The resistance of the slab could not be determined, because it is of the same order as the noise in the signals. The noise is this large because the peak load and the inertia forces are some orders higher than the resistance. This points out the limits of the test method. By using more stable measurement equipment, and by using explosives with a lower detonation velocity, the problem can be reduced, but it cannot be eliminated.

5 Conclusions

Blast tests were performed on seven simply supported reinforced concrete slabs. The loading was generated by four identical explosive charges. The slabs had the following dimensions: length of 1.2 m, support length of 1.1 m, width of 0.85 m and thickness of 125 mm. They were all reinforced with longitudinal and transverse reinforcement. Three of them also had lacing reinforcement. The slabs were brought to failure in either one or two shocks.

After the tests, it appeared that the applied load was not uniformly distributed and that the displacement signals were highly disturbed by the flash of the explosion, which obscured the beginning of these measurements. Yet, it was possible to draw the resistance-deformation curves of the slabs in the final stage of the deformation process up to failure. From these curves, the ultimate deformation at failure could be estimated. Unfortunately, the maximum resistance could not be determined since its value was in the order of the noise level in the signals.

Analysis and comparison of the present and previous tests led to the following conclusions.

- 1 The presence of thick longitudinal reinforcement rods notably increases the deformation capacity of the slabs.
- 2 Lacing increases the deformation capacity if otherwise the slab would have failed in the compression zone. Lacing prevents failure in the compression zone and the failure mode changes to tensile failure. Hence, lacing is only useful when failure would have occurred in the compression zone.
- 3 The empirical relationship established in previous test series is only applicable for compressive failure of the slabs.
- 4 Another relationship has been established in this test series for tensile failure of the slabs.
- 5 The impulsive character of the shock load in the present test does not change the behaviour of the slab. With regard to the deformation capacity, the results do match.

A comparison of the test results with a calculation according to the design rules of TM 5-1300 showed that the ultimate support rotation of the slabs without shear reinforcement is considerably higher than the value prescribed by TM 5-1300. This corresponds with the results of previous tests. For the slabs with lacing, the values prescribed by the design manual are too high. Tensile failure occurred sooner than at 12 degrees support rotation. Thus, TM 5-1300 should be used carefully.

Some improvements in the test method are suggested in this report. Furthermore, application of the test method under very high shock loadings is advised against. In the present tests, the order of the resistance of the slab was in the same order as the

noise in the measurement signals. Therefore, it was not possible to determine the maximum resistance of the slab.

For the next phase of the project, the following proposition is made: perform tests with a different thickness of slab or different material properties to extend or demarcate the field of validity of both empirical relationships. Especially validation of the tensile failure criterion is necessary, because of the many problems which were encountered in the present test series.

It is advised to study the test set-up carefully before performing new tests, in order to solve the problems which are encountered.

New tests should be combined with numerical simulations in order to diminish the number of necessary experiments.

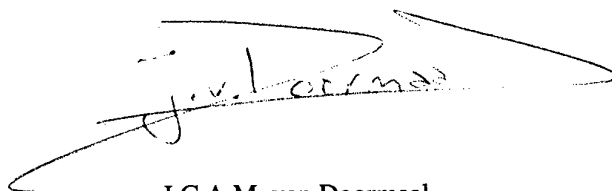
6 References

- [1] Doormaal, J.C.A.M. van,
Dynamic deformation capacity of reinforced concrete.
Phase 2 - Test method,
TNO Prins Maurits Laboratory, PML 1995-A24,
Rijswijk, May 1995.
- [2] Doormaal, J.C.A.M. van,
Dynamic deformation capacity of reinforced concrete.
Phase 3 - Experiments on simply supported slabs,
TNO Prins Maurits Laboratory, PML 1995-A82,
Rijswijk, December 1995.
- [3] Doormaal, J.C.A.M. van,
Dynamic deformation capacity of reinforced concrete.
Phase 4 - Influence of shear reinforcement,
TNO Prins Maurits Laboratory, PML 1996-A76,
Rijswijk, January 1997.
- [4] Doormaal, J.C.A.M. van,
Dynamische vervormingscapaciteit van gewapend beton.
Fase 1: Literatuuronderzoek,
TNO Prins Maurits Laboratory, PML 1993-24,
Rijswijk, 1993.
- [5] TM 5-1300,
Departments of the American Army, the Navy and the Air Force,
Structures to resist the effect of accidental explosives,
Washington DC, 19 November 1991.
- [6] Wees, R.M.M. van and Kastele, R.M. van de,
Scaled blast experiments for the reaction frame,
TNO Prins Maurits Laboratory, PML 1997-IN4,
Rijswijk, 1997.
- [7] Timoshenko, S.; Young, D.H. and Weaver, W.,
Vibration Problems in Engineering,
Fourth edition, New York.

7 Authentication

A stylized handwritten signature consisting of a large 'J' and a horizontal line.

Dr. J. Weerheijm
Group leader

A handwritten signature that appears to read 'J.C.A.M. van Doormaal' in a cursive script.

J.C.A.M. van Doormaal
Author/Project leader

Annex A Concrete composition

The concrete mix was made in accordance with the VBT 1986 (NEN 5950). It consists of furnace cement and river sand. A gradation of the aggregates around line B8 (i.e. maximum aggregate size of 8 mm) was realised with common concrete sand, an addition of 4 mm aggregates and of aggregates smaller than 0.25 mm. A superplastificator (1% m/m Betomix 450) has been added in order to obtain the desired concrete quality. Table A.1 gives the casting data for two slabs (numbers 1 and 5), which are representative of the other slabs.

Table A.1: Casting data of concrete.

Casting date	12-03-1997	12-03-1997
Setting measure NEN 5956 (mm)	29	32
Shaking measure NEN 5957 (mm)	320	320
Volumic mass NEN 5959 (kg/m ³)	2207	2193
Air content NEN 5962 (%(V/V))	6.2	6.8
Cement content at wcf 0.55 (kg/m ³)	317	315
Slab number	1	7

The slabs and the specimens for the material tests were densified and after-cured as follows:

- the concrete was densified with a vibrating needle per reinforcement mesh;
- the slab was made smooth using a vibrating beam and finished with a hand skimmer;
- the slabs were covered with plastic foil for six days, and then exposed to the air for 28 days.

The material tests gave the mechanical properties as presented in Table A.2.

Table A.2: Mechanical properties of concrete.

Slab numbers	Age	Cube strength (MPa)	Splitting tensile strength (MPa)	Young's Modulus (GPa)
1 to 3	28	42.1	3.30	30.3
4 to 7	28	41.8	3.12	31
3	28+12	43.0	3.30	30.3
7	28+12	39.4	3.12	31
4	28+14	40.3	3.12	31
6	28+14	43.9	3.12	31
5	28+19	36.8	3.12	31
1	28+28	40.5	3.30	30.3
2	28+28	38.8	3.30	30.3

Annex B Calculations and predictions

B.1 Determination of the amount of charge

The determination of the amount of charge was an iterative process.

- 1 An amount of explosive (KNEED no. 6) is chosen.
- 2 The location with regard to the slab is given (see section 2.3).
- 3 The characteristics of the shock load are calculated according to [6].
- 4 The slab is modelled as a mass-spring system. The equation of motion is then solved. This provides the theoretical maximum deflection under the calculated load.
- 5 The calculated maximum deflection is compared with the estimated ultimate deflection of the slab at which it is expected to fail. If the maximum deflection is slightly larger than the estimated deflection, then the amount of explosive is used for the experiments. If not, another amount has to be chosen, and the calculations have to be done again.

B.2 Calculations of the shock characteristics

The characteristics of the shock load are calculated according to [6]. The method in this report is based on the curve-fits from AASTP-1 [AC/258, 1992] for single free-air TNT charges. Multiplication factors are given to find the shock characteristics for four free-air charges:

- the factor for the reflected peak overpressure is given as 1.8;
- the factor for the reflected impulse is given as 2.5.

B.3 Modelisation of slab types 4.1.1 and 4.1.2

The studied slabs have these dimensions:

length of the slab:	L_o	= 1200 mm
support length:	L	= 1100 mm
loaded length:	L_p	= 1000 mm
width:	B	= 850 mm
height:	T	= 125 mm

The reinforcement is symmetric (both sides equally reinforced) and its other characteristics are:

diameter on the tensile side:	ϕ_1	= 8 mm
diameter on the compressive side:	ϕ_2	= 8 mm
diameter in transverse direction:	ϕ_t	= 8 mm

in-between distance:	b	$= 130 \text{ mm}$
number of rods:	n_b	$= 7$
concrete cover on the tensile side:	c_p	$= 15 \text{ mm}$
concrete cover on the compressive side:	c_n	$= 15 \text{ mm}$
effective depth on the tensile side:	d_p	$= T - c_p - 0.5 \cdot \phi_1 - \phi_t$
	d_p	$= 0.098 \text{ m}$
effective depth on the compressive side:	d_n	$= T - c_n - 0.5 \cdot \phi_2 - \phi_t$
	d_n	$= 0.098 \text{ m}$
average effective depth:	d_a	$= (d_p + d_n) / 2$
area of tension reinforcement:	A_{s1}	$= (\pi \cdot \phi_1^2) / 4$
	A_{s1}	$= 5.02655 \text{e-5 m}^2$
area of compression reinforcement:	A_{s2}	$= (\pi \cdot \phi_2^2) / 4$
	A_{s2}	$= 5.02655 \text{e-5 m}^2$
amount of reinforcement		
-on the tensile side:	p_p	$= A_{s1} / (b \cdot d_p)$
	p_p	$= 0.00395$
-on the compressive side:	p_n	$= A_{s2} / (b \cdot d_n)$
	p_n	$= 0.00395$
	p	$= n_b \cdot A_{s1} / (B \cdot d_p)$
	p	$= 0.00422$
	p_p	$= p_n = p$
average reinforcement ratio:	p_a	$= (p_p + p_n) / 2$
	p_a	$= 0.00422$

The properties of the steel reinforcement, as specified by the manufacturer, are:

yield strength:	f_y	$= 500.10^6 \text{ Pa}$
ultimate strength:	f_u	$= 580.10^6 \text{ Pa}$
Young's modulus:	E_s	$= 210.10^9 \text{ Pa}$

The value given for the steel yield strength is usually a minimum value and can often be increased by 10%. This is the reason why the more realistic value $f_y = 550.10^6 \text{ Pa}$ will be used in the calculations.

The properties of concrete, measured on concrete samples, are:

cube strength:	f_c	$= 40.7 \text{ MPa}$
Young's modulus:	E_c	$= 30.9 \text{ GPa}$
Poisson's ratio:	ν	$= 0.167$

Table 4.1 of TM 5-1300 gives the following dynamic increase factors to be used in the calculations of slabs in bending:

concrete, bending:	DIF_{bb}	$= 1.19$
concrete, direct shear:	DIF_{ba}	$= 1.10$
yield strength, bending:	DIF_{vb}	$= 1.17$
ultimate strength, bending:	DIF_{tb}	$= 1.05$
yield strength, direct shear:	DIF_{va}	$= 1.10$

ultimate strength, direct shear:

$$DIF_{ta} = 1.00$$

Thus, the dynamic strength properties can be deduced:

concrete, bending:

$$\begin{aligned} f_{dc} &= DIF_{bb}.f_c \\ f_{dc} &= 4.8433.e7 \text{ kg.m}^{-1}.\text{sec}^{-2} \end{aligned}$$

yield strength, bending:

$$\begin{aligned} f_{dy} &= DIF_{vb}.f_y \\ f_{dy} &= 6.435.e8 \text{ kg.m}^{-1}.\text{sec}^{-2} \end{aligned}$$

ultimate strength, bending:

$$\begin{aligned} f_{du} &= DIF_{tb}.f_u \\ f_{du} &= 6.09.e8 \text{ kg.m}^{-1}.\text{sec}^{-2} \end{aligned}$$

According to Table 4.2 in TM 5-1300, the dynamic design stress for the reinforcement can be taken as:

$$\begin{aligned} f_{ds} &= (f_{du} + f_{dy})/2 \\ f_{ds} &= 6.2625.e8 \text{ kg.m}^{-1}.\text{sec}^{-2} \end{aligned}$$

The ultimate resisting moment can now be calculated with the formula:

-on the tensile side:

$$\begin{aligned} M_p &= B.p_p.d_p.f_{ds}.(d_p - a_p/2) + B.p_p.d_p.f_{ds}.(d_p - d_1 - a_p/2) \\ M_p &= 2.61564.e4 \text{ kg.m}^2.\text{sec}^{-2} \end{aligned}$$

-on the compressive side:

$$\begin{aligned} M_n &= B.p_n.d_n.f_{ds}.(d_n - a_n/2) + B.p_n.d_n.f_{ds}.(d_n - d_1 - a_n/2) \\ M_n &= 2.61564.e4 \text{ kg.m}^2.\text{sec}^{-2} \end{aligned}$$

where the depth of equivalent rectangular stress blocks is:

-on the tensile side:

$$\begin{aligned} a_p &= (p_p.d_p.f_{ds})/(0.85.f_{dc}) \\ a_p &= 6.29704 \text{ mm} \end{aligned}$$

-on the compressive side:

$$\begin{aligned} a_n &= (p_n.d_n.f_{ds})/(0.85.f_{dc}) \\ a_n &= 6.29704 \text{ mm} \end{aligned}$$

and the distance between compression and tensile steel is:

$$\begin{aligned} d_1 &= d_p - 0.5.\phi_1 - c_n - \phi_t \\ d_1 &= 0.071 \text{ m} \end{aligned}$$

The above formula for the ultimate resisting moment is used because this is a conservative approach for the prediction of the maximum deformation. The crushing and the spalling of concrete is neglected: the slab concrete cross-section is a cross-section type 1.

In the calculation, the average moment of inertia of the concrete cross-section is used, which is given by:

$$I_a = ((I_g + I_c).B)/2$$

where:

moment of inertia of the gross concrete cross-section:

$$I_g = (T^3)/12$$

moment of inertia of the cracked concrete cross-section:

$$I_c = F.d_a^3$$

coefficient given in Figures 4-12 of TM 5-1300:

$$F = 0.0198$$

This coefficient depends on the percentage of reinforcement ($p=0.00422$) and on the modular ratio ($n=6.796$).

The maximum resistance of a simply supported slab is given by:

$$\begin{aligned} \text{ultimate unit resistance:} \quad r_u &= 8.M_p/(L^2.B) \\ &= 2.03452e5 \text{ MPa} \\ \text{total ultimate resistance:} \quad R_u &= B.L.r_u \\ &= 1.90228e5 \text{ N} \end{aligned}$$

The elastic resistance of a simply supported slab is:

$$\begin{aligned} \text{elastic resistance:} \quad r_e &= 8.M_p/(B.L^2) \\ &= 2.03452e5 \text{ Pa} \end{aligned}$$

The stiffness can be calculated as follows:

$$\begin{aligned} \text{effective elastic stiffness:} \quad k_E &= 384 E_c I_a / (5.L^3) \\ &= 1.37454e8 \text{ kg.sec}^{-2} \end{aligned}$$

And the maximum elastic deflection can then be determined:

$$\begin{aligned} \text{maximum elastic deflection:} \quad X_E &= (r_u.B.L)/k_E \\ &= 1.38394 \text{ mm} \end{aligned}$$

The load mass factors are given in Table 3.12 of TM 5-1300:

$$\begin{aligned} \text{in the elastic range} \quad KLM_e &= 0.78 \\ \text{in the plastic range} \quad KLM_p &= 0.66 \\ \text{The average is} \quad KLM &= (KLM_e + KLM_p)/2 \\ &= 0.715 \end{aligned}$$

Using the average load-mass factor, the equivalent mass for the system is found:

$$\begin{aligned} \text{the mass of the element between its supports is:} \quad M &= 294.6 \cdot 11/12 \\ &= 270 \text{ kg} \\ M_{eq} &= KLM.M \\ &= 193.0 \text{ kg} \end{aligned}$$

$$\begin{aligned} \text{the natural period is eventually equal to:} \quad T_N &= 2.\pi.\sqrt{(M_{eq}/K_E)} \\ &= 0.0075 \text{ sec} \end{aligned}$$

Check now the shear strength of the slab. The shear capacity of concrete with longitudinal reinforcement equals:

$$v_c = 0.158.f_{dc}^{0.5} + 17.24.Pa$$

The dynamic increase factor for the strength properties of concrete under shear loading is equal to 1.10. So, in this case, one must calculate with a dynamic cube strength of:

$$\begin{aligned} f_{dc} &= 1.10.f_c \\ &= 44.77 \text{ MPa} \end{aligned}$$

and the shear capacity is then found to be:

$$v_c = 1.13 \text{ MPa}$$

The maximum shear stress that can occur in the present loading situation equals:

$$v_u = [R_u.(L/2-d)]/[L.B.d]$$

where:

d: effective depth ($d=d_n=d_p$)

L: support length

The maximum shear stress is, then:

$$v_u = 0.938 \text{ MPa}$$

The ultimate shear stress is lower than the shear capacity. This indicates that the slab should not fail due to shear. For slabs with lacing, the shear capacity is higher. Therefore, the same conclusion can be drawn.

B.4 Modelling of slab types 4.2.1 and 4.2.2

The studied slabs have these dimensions:

length of the slab:	L_o	= 1200 mm
support length:	L	= 1100 mm
loaded length:	L_p	= 1000 mm
width:	B	= 850 mm
height:	T	= 125 mm

The reinforcement is symmetric (both sides equally reinforced) and its other characteristics are:

diameter on the tensile side:	ϕ_1	= 10 mm
diameter on the compressive side:	ϕ_2	= 10 mm
diameter in transverse direction:	ϕ_t	= 8 mm
in-between distance:	b	= 175 mm
number of rods:	nb	= 5
concrete cover on the tensile side:	c_p	= 15 mm
concrete cover on the compressive side:	c_n	= 15 mm
effective depth on the tensile side:	d_p	= $T - c_p - 0.5 \cdot \phi_1 - \phi_t$
	d_p	= 0.097 m
effective depth on the compressive side:	d_n	= $T - c_n - 1.5 \cdot \phi_2 - \phi_t$
	d_n	= 0.097 m
average effective depth:	d_a	= $(d_p + d_n)/2$
	d_a	= 0.097 m
area of tension reinforcement:	A_{s1}	= $(\pi \cdot \phi_1^2)/4$
	A_{s1}	= $7.85398e-5 \text{ m}^2$
area of compression reinforcement:	A_{s2}	= $(\pi \cdot \phi_2^2)/4$
	A_{s2}	= $7.85398e-5 \text{ m}^2$
amount of reinforcement on the tensile side:	p_p	= $A_{s1}/(b \cdot d_p)$
	p_p	= 0.00463
amount of reinforcement on the compressive side:	p_n	= $A_{s2}/(b \cdot d_n)$
	p_n	= 0.00463
	p	= $nb \cdot A_{s1}/(B \cdot d_p)$
	p	= 0.00476
	p_p	= $p_n = p$

$$\begin{aligned}\text{average reinforcement ratio:} \quad p_a &= (p_p + p_n)/2 \\ p_a &= 0.00476\end{aligned}$$

The properties of the steel reinforcement, as specified by the manufacturer, are:

$$\begin{aligned}\text{yield strength:} \quad f_y &= 500.10^6 \text{ Pa} \\ \text{ultimate strength:} \quad f_u &= 580.10^6 \text{ Pa} \\ \text{Young's modulus:} \quad E_s &= 210.10^9 \text{ Pa}\end{aligned}$$

The value given for the steel yield strength is usually a minimum value and can often be increased by 10%. This is the reason why the more realistic value $f_y = 550.10^6 \text{ Pa}$ will be used in the calculations.

The properties of concrete, measured on concrete samples, are:

$$\begin{aligned}\text{cube strength:} \quad f_c &= 39.7 \text{ MPa} \\ \text{Young's modulus:} \quad E_c &= 30.3 \text{ GPa} \\ \text{Poisson's ratio:} \quad \nu &= 0.167\end{aligned}$$

Table 4.1 of TM 5-1300 gives the following dynamic increase factors to be used in the calculations of slabs in bending:

$$\begin{aligned}\text{concrete, bending:} \quad \text{DIF}_{bb} &= 1.19 \\ \text{concrete, direct shear:} \quad \text{DIF}_{ba} &= 1.10 \\ \text{yield strength, bending:} \quad \text{DIF}_{vb} &= 1.17 \\ \text{ultimate strength, bending:} \quad \text{DIF}_{tb} &= 1.05 \\ \text{yield strength, direct shear:} \quad \text{DIF}_{va} &= 1.10 \\ \text{ultimate strength, direct shear:} \quad \text{DIF}_{ta} &= 1.00\end{aligned}$$

Thus, the dynamic strength properties can be deduced:

$$\begin{aligned}\text{concrete, bending:} \quad f_{dc} &= \text{DIF}_{bb} \cdot f_c \\ f_{dc} &= 4.7243 \cdot 10^7 \text{ kg.m}^{-1}.\text{sec}^{-2} \\ \text{yield strength, bending:} \quad f_{dy} &= \text{DIF}_{vb} \cdot f_y \\ f_{dy} &= 6.435 \cdot 10^8 \text{ kg.m}^{-1}.\text{sec}^{-2} \\ \text{ultimate strength, bending:} \quad f_{du} &= \text{DIF}_{tb} \cdot f_u \\ f_{du} &= 6.09 \cdot 10^8 \text{ kg.m}^{-1}.\text{sec}^{-2}\end{aligned}$$

According to Table 4.2 in TM 5-1300, the dynamic design stress for the reinforcement can be taken as:

$$\begin{aligned}f_{ds} &= (f_{du} + f_{dy})/2 \\ f_{ds} &= 6.2625 \cdot 10^8 \text{ kg.m}^{-1}.\text{sec}^{-2}\end{aligned}$$

The ultimate resisting moment can now be calculated with the formula:

-on the tensile side:

$$\begin{aligned}M_p &= B \cdot p_p \cdot d_p \cdot f_{ds} \cdot (d_p - a_p/2) + B \cdot p_n \cdot d_p \cdot f_{ds} \cdot (d_p - d_1 - a_p/2) \\ M_p &= 2.89691 \cdot 10^4 \text{ kg.m}^2.\text{sec}^{-2}\end{aligned}$$

-on the compressive side:

$$\begin{aligned}M_n &= B \cdot p_n \cdot d_n \cdot f_{ds} \cdot (d_n - a_n/2) + B \cdot p_p \cdot d_n \cdot f_{ds} \cdot (d_n - d_1 - a_n/2) \\ M_n &= 2.89691 \cdot 10^4 \text{ kg.m}^2.\text{sec}^{-2}\end{aligned}$$

where the depth of equivalent rectangular stress blocks is:

-on the tensile side:

$$a_p = (p_p \cdot d_p \cdot f_{ds}) / (0.85 \cdot f_{dc})$$

$$a_p = 7.20497 \text{ mm}$$

-on the compressive side:

$$a_n = (p_n \cdot d_n \cdot f_{ds}) / (0.85 \cdot f_{dc})$$

$$a_n = 7.20497 \text{ mm}$$

and the distance between compression and tensile steel is:

$$d_1 = d_p - 0.5 \cdot \phi_1 - c_n - \phi_t$$

$$d_1 = 0.069 \text{ m}$$

The above formula for the ultimate resisting moment is used because this is a conservative approach for the prediction of the maximum deformation. So, the crushing and the spalling of concrete is neglected: the slab concrete cross-section is a cross-section type 1.

In the calculation, the average moment of inertia of the concrete cross-section is used, which is given by :

$$I_a = ((I_g + I_c) \cdot B) / 2$$

where:

moment of inertia of the gross concrete cross-section: $I_g = T^3 / 12$

moment of inertia of the cracked concrete cross-section: $I_c = F \cdot d \cdot a^3$

coefficient given in Figures 4-12 of TM 5-1300: $F = 0.0223$

This coefficient depends on the percentage of reinforcement ($p=0.00476$) and on the modular ratio ($n=6.93069$).

The maximum resistance of a simply supported slab is given by:

ultimate unit resistance: $r_u = 8 \cdot M_p / (L^2 \cdot B)$

$$r_u = 2.25331 \text{e5 Pa}$$

total ultimate resistance: $R_u = B \cdot L \cdot r_u$

$$R_u = 2.10684 \text{e5 N}$$

The elastic resistance of a simply supported slab is:

elastic resistance: $r_e = 8 \cdot M_p / (B \cdot L^2)$

$$r_e = 2.25331 \text{e5 Pa}$$

The stiffness can be calculated as follows:

effective elastic stiffness: $k_E = 384 E_c \cdot I_a / (5 \cdot L^3)$

$$k_E = 1.36061 \text{e8 N} \cdot \text{m}^{-1}$$

And the maximum elastic deflection can then be determined:

maximum elastic deflection: $X_E = (r_u \cdot B \cdot L) / k_E$

$$X_E = 1.548 \text{ mm}$$

The load mass factors are given in Table 3.12 of TM 5-1300:

in the elastic range $KLMe = 0.78$

in the plastic range $KLMp = 0.66$

The average is:

$$KLM = (KLMe + KLMp) / 2$$

$$KLM = 0.715$$

Using the average load-mass factor, the equivalent mass for the system is found:

$$\begin{aligned} \text{the mass of the element between its supports is: } M &= 294 \cdot 11/12 \\ M &= 270 \text{ kg} \\ M_{eq} &= KLM \cdot M \\ M_{eq} &= 193 \text{ kg} \end{aligned}$$

$$\begin{aligned} \text{The natural period is eventually equal to: } T_N &= 2\pi \cdot \sqrt{(M_{eq}/K_E)} \\ T_N &= 0.0075 \text{ sec} \end{aligned}$$

Check now the shear strength of the slab. The shear capacity of concrete with longitudinal reinforcement equals:

$$v_c = 0.158 \cdot f_{dc}^{0.5} + 17.24 \cdot Pa$$

The dynamic increase factor for the strength properties of concrete under shear loading is equal to 1.10. So, in this case, one must calculate with a dynamic cube strength of:

$$\begin{aligned} f_{dc} &= 1.10 \cdot f_c \\ f_{dc} &= 43.67 \text{ MPa} \end{aligned}$$

and the shear capacity is then found to be:

$$v_c = 1.126 \text{ MPa}$$

The maximum shear stress that can occur in the present loading situation equals:

$$v_u = [R_u \cdot (L/2 - d)] / [L \cdot B \cdot d]$$

where:

d: effective depth ($d = d_n = d_p$)

L: support length

Therefore, the maximum shear stress is:

$$v_u = 1.05 \text{ MPa}$$

The ultimate shear stress is lower than the shear capacity. This indicates that the slab should not fail due to shear. For slabs with lacing, the shear capacity is higher. Thus, the same conclusion can be drawn.

B.5 Summary of results

The load characteristics are calculated and next the response of the slab for several charges. The results of these calculations are summarised in Tables B.1 and B.2.

Table B.1: Prediction of maximum deformation of slabs 4.1.1 and 4.1.2.

1 charge W (kg)	4 charges Wtot (kg)	R (m)	T _p (s)	P (N)	θ (°)
0.5	2	0.550	1.6035e-4	2.0905e7	3.2
0.6	2.4	0.550	1.5927 e-4	2.0676 e7	3.7
0.65	2.6	0.550	1.5907 e-4	2.2065 e7	4.2
0.7	2.8	0.550	1.5903 e-4	2.3415 e7	4.8
0.75	3	0.550	1.5913 e-4	2.473 e7	5.3
0.8	3.2	0.550	1.5934 e-4	2.601e7	5.9
0.85	3.4	0.550	1.5963 e-4	2.7259 e7	6.4
0.9	3.6	0.550	1.5999 e-4	2.8478 e7	7.1
0.95	3.8	0.550	1.6041 e-4	2.9669 e7	7.7
1	4	0.550	1.6088 e-4	3.0833 e7	8.3
1.05	4.2	0.550	1.6139 e-4	3.1973 e7	9
1.1	4.4	0.550	1.6194 e-4	3.3089 e7	9.7
1.15	4.6	0.550	1.6252 e-4	3.4182 e7	10.4
1.2	4.8	0.550	1.6312 e-4	3.5255 e7	11.1
1.25	5	0.550	1.6374 e-4	3.6307 e7	11.8
1.3	5.2	0.550	1.6438 e-4	3.734 e7	12.6
1.35	5.4	0.550	1.6503 e-4	3.8355 e7	13.4
1.4	5.6	0.550	1.657 e-4	3.9352 e7	14.2

Table B.2: Prediction of maximum deformation of slabs 4.2.1 and 4.2.2.

1 charge W (kg)	4 charges Wtot (kg)	R (m)	T _p (s)	P (N)	θ (°)
0.5	2	0.550	1.6035e-4	2.0905e7	3
0.6	2.4	0.550	1.5927 e-4	2.0676 e7	3.4
0.65	2.6	0.550	1.5907 e-4	2.2065 e7	3.8
0.7	2.8	0.550	1.5903 e-4	2.3415 e7	4.3
0.75	3	0.550	1.5913 e-4	2.473 e7	4.8
0.8	3.2	0.550	1.5934 e-4	2.601e7	5.3
0.85	3.4	0.550	1.5963 e-4	2.7259 e7	5.8
0.9	3.6	0.550	1.5999 e-4	2.8478 e7	6.4
0.95	3.8	0.550	1.6041 e-4	2.9669 e7	6.9
1	4	0.550	1.6088 e-4	3.0833 e7	7.5
1.05	4.2	0.550	1.6139 e-4	3.1973 e7	8.1
1.1	4.4	0.550	1.6194 e-4	3.3089 e7	8.8
1.15	4.6	0.550	1.6252 e-4	3.4182 e7	9.4
1.2	4.8	0.550	1.6312 e-4	3.5255 e7	10
1.25	5	0.550	1.6374 e-4	3.6307 e7	10.7
1.3	5.2	0.550	1.6438 e-4	3.734 e7	11.4
1.35	5.4	0.550	1.6503 e-4	3.8355 e7	12.1
1.4	5.6	0.550	1.657 e-4	3.9352 e7	12.8

Annex C Shock load

In Table C.1, the measured shock load P1 in test 1 on slab 7 is given as an example. The influence of each charge can be seen clearly on this loading curve. The arrival of four shock waves are visible. The arrival times of each of the four charges on the slab correspond well with the predicted arrival times, based on single charge calculations.

Table C.1: Measured shock load P1 in test 1 on slab 7.

	Predicted arrival time (ms)	Measured arrival time (ms)	Error (%)
peak 1	0.207	0.230	10
peak 2	0.280	0.269	4.1
peak 3	0.389	0.313	24.3
peak 4	0.460	0.357	28.9

N.B.: the arrival time is calculated from the moment of detonation ($t_0=4.083\text{ms}$).

The increasing difference between the predicted values and those measured is not surprising, because the calculations were done for free-air charges. For a combination of four charges, the arrival times are not exactly the same. The load generated by the charge nearest to the pressure transducer arrives at time t_1 as if it were a free-air charge, because it crosses a medium which is not disturbed. But this is not the case for the shock waves coming from the other charges: they travel through a compressed medium generated by the shock waves arriving sooner. This results in higher speeds of the shock waves. The arrival times for the corresponding shock waves are thus shorter than the predicted arrival times.

The presence of a fifth peak on the loading is strange. In fact, it cannot be due to a shock load; first because its presence is not detected by the pressure transducer at location P2; secondly because it is twice as high as than the other peaks; and thirdly because its form is much smoother than the other peaks. Its presence may be due to something hitting the slab, such as a piece of concrete or one of the iron bars holding the explosive charges.

For the other tests, the measured pressure load P1 can be analysed similarly, although the four shock waves are not always as easy to discern as in this test. With larger charges, the difference in arrival time diminishes. Furthermore, the detonation of the four charges will not be exactly simultaneous, and will be different in every test.

The fact that the four shock waves can be discerned at the location of measurement points out that the shock load cannot be uniformly distributed. At other locations, the shock loads will arrive at other points in time.

From the impulse point of view, the distribution over the slab appears to be more uniform. This follows from the comparison between the measured impulses and the predicted impulses. This comparison is given in Table C.2. It can be seen that the impulse measured is of the same order as the predicted impulse, even if the

measured and predicted peak pressure differ considerably. The impulse of the load at P2 is smaller because this point lies outside the region of 'uniform' shock load.

Table C.2: Comparison of load characteristics with predictions.

Test	1	2	9	3	5
Charge (kg)	3.4	3.4	3.4	3	3
Measured peak pressure at location P1 (bar)	139.7	95.6	214.7	224	82
Measured peak pressure at location P2 (bar)	147	-	163	250	137
Predicted peak pressure (bar)	320.8	320.8	320.8	290.9	290.9
Measured impulse at location P1 (Pa.sec)	1862	1394	2528	2097	1509
Measured impulse at location P2 (Pa.sec)	1098	-	1175	1478	1051
Predicted impulse (Pa.sec)	2560	2560	2560	2315	2315

Test	4	7	6	10	8
Charge (kg)	5	5	2	2	4.4
Measured peak pressure at location P1 (bar)	390	-	136	185.4	378.7
Measured peak pressure at location P2 (bar)	115	182	88	107	140
Predicted peak pressure (bar)	427.1	427.1	209.1	209.1	389.3
Measured impulse at location P1 (Pa.sec)	2528	-	1726	1621	3980
Measured impulse at location P2 (Pa.sec)	1175	1723	754	905.4	1414
Predicted impulse (Pa.sec)	3497	3497	1676	1676	3152

Annex D Manipulation of the measured signals

We have obtained ten signals:

- the pressure at location P1;
- the pressure next to the slab P2;
- the pressure underneath the slab P3;
- four displacements at locations D1, D2, D3 and D4;
- three accelerations at locations A2, A3 and A4.

The displacement measurements are disturbed too long by the flash of the explosion. This makes them useless for most of the tests. Only for the tests in which the slabs did not fail, can the end deformation be read from the signals.

The resistance-deformation curve has therefore been determined using only the acceleration measurements and the pressure measurements. By integrating the accelerations twice, an estimation of the displacement has been obtained.

Two observations were made about the deformation of the slab.

- The third mode was hit and cannot be neglected, especially not in the acceleration. Thanks to orthogonality, the two modes can be treated separately as long as they do not interact (see ref. [7]). Since the third mode damps out and stays elastic (see Figure D.1), it can be assumed that the use of orthogonality is correct. The measured displacements and accelerations must be split up into the two modes.
- The plastic deformation shape resembles the elastic deformation shape of the first mode. There is not a single hinge, but a large plastic zone. This is shown for the end deformation of the slabs in test 2, test 5 and test 9 in Figures D.2 to D.4. In these tests, the slabs did not fail.

As a consequence, the elastic and plastic deformation cannot be separated.

The theoretical shape functions for splitting up the deformation and acceleration are given by:

$$\phi_{m1} = \frac{16}{5} \left(\frac{x}{L} \right)^4 - \frac{24}{5} \left(\frac{x}{L} \right)^2 + 1$$

$$\phi_{m3} = -\sin\left(\frac{3\pi x}{L}\right)$$

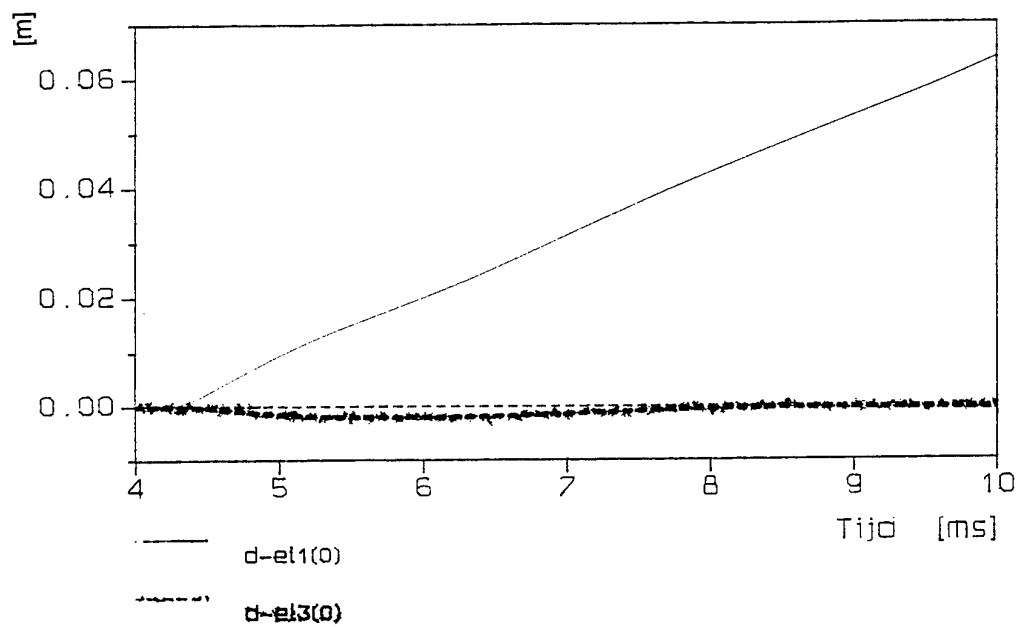


Figure D.1: Splitting up of the displacement signals (from integrated acceleration) into the first ($d-el1(0)$) and third mode ($d-el3(0)$), test 1- slab 7.

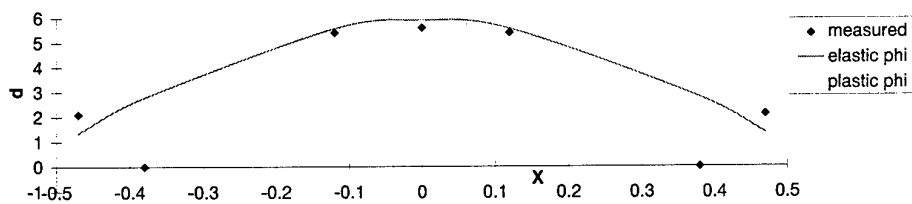


Figure D.2: Comparison of deformation of slab 3 after test 2 with the theoretical elastic and plastic shape functions.

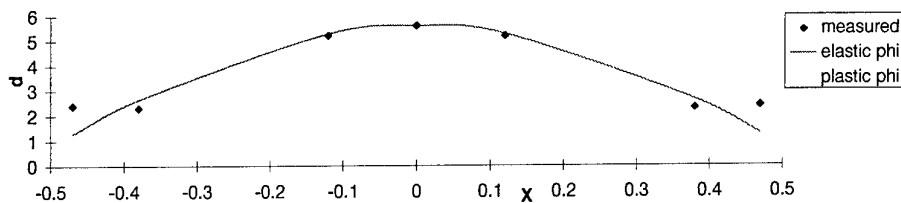


Figure D.3: Comparison of deformation of slab 6 after test 5 with the theoretical elastic and plastic shape functions.

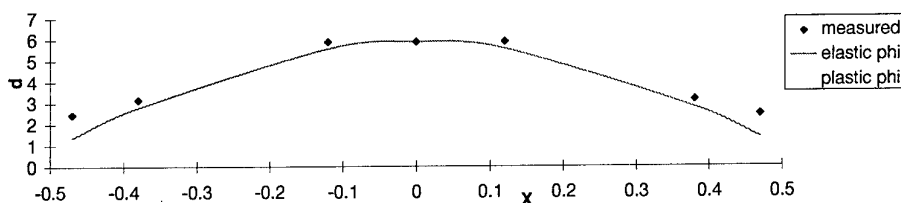


Figure D.4: Comparison of deformation of slab 5 after test 9 with the theoretical elastic and plastic shape functions.

The set of equations for splitting up the displacement and the acceleration is given by:

$$\begin{bmatrix} d(D1) \\ d(D2) \\ d(D3) \\ d(D4) \end{bmatrix} = \begin{bmatrix} \phi_{m1}(x_{d1}) & \phi_{m3}(x_{d1}) \\ \phi_{m1}(x_{d2}) & \phi_{m3}(x_{d2}) \\ \phi_{m1}(x_{d3}) & \phi_{m3}(x_{d3}) \\ \phi_{m1}(x_{d4}) & \phi_{m3}(x_{d4}) \end{bmatrix} \begin{bmatrix} d_{m1}(0) \\ d_{m3}(0) \end{bmatrix}$$

$$\begin{bmatrix} a(A2) \\ a(A3) \\ a(A4) \end{bmatrix} = \begin{bmatrix} \phi_{m1}(x_{a2}) & \phi_{m3}(x_{a2}) \\ \phi_{m1}(x_{a3}) & \phi_{m3}(x_{a3}) \\ \phi_{m1}(x_{a4}) & \phi_{m3}(x_{a4}) \end{bmatrix} \begin{bmatrix} a_{m1}(0) \\ a_{m3}(0) \end{bmatrix}$$

The inverses can be calculated of the least square method:

$$\begin{bmatrix} d_{m1}(0) \\ d_{m3}(0) \end{bmatrix} = \begin{bmatrix} 0.233 & 0.412 & 0.357 & 0.425 \\ 0.315 & -0.059 & -0.259 & 0.514 \end{bmatrix} \begin{bmatrix} d(D1) \\ d(D2) \\ d(D3) \\ d(D4) \end{bmatrix}$$

$$\begin{bmatrix} a_{m1}(0) \\ a_{m3}(0) \end{bmatrix} = \begin{bmatrix} 0.444 & 0.418 & 0.372 \\ 0.117 & -0.427 & 0.593 \end{bmatrix} \begin{bmatrix} a(A2) \\ a(A3) \\ a(A4) \end{bmatrix}$$

In test 1 and test 10, measurement D2 failed and so cannot be used in the analysis. The set of equations is then given by:

$$\begin{bmatrix} d_{m1}(0) \\ d_{m3}(0) \end{bmatrix} = \begin{bmatrix} 0.274 & 0.691 & 0.521 \\ 0.309 & -0.308 & 0.50 \end{bmatrix} \begin{bmatrix} d(D1) \\ d(D3) \\ d(D4) \end{bmatrix}$$

In test 2, measurement D4 failed and therefore cannot be used in the analysis. The set of equations is then given by:

$$\begin{bmatrix} d_{m1}(0) \\ d_{m3}(0) \end{bmatrix} = \begin{bmatrix} 0.856 & 0.611 & 0.226 \\ 1.068 & 0.182 & -0.418 \end{bmatrix} \begin{bmatrix} d(D1) \\ d(D2) \\ d(D3) \end{bmatrix}$$

In tests 2, 4, 6, 7 and 9, measurement A4 failed and so cannot be used in the analysis. The set of equations is then given by:

$$\begin{bmatrix} a_{m1}(0) \\ a_{m3}(0) \end{bmatrix} = \begin{bmatrix} 1.079 & 0.075 \\ 1.129 & -0.974 \end{bmatrix} \begin{bmatrix} a(A2) \\ a(A3) \end{bmatrix}$$

The resistance of the slab follows from the equation of motion:

$$R(t) = F(t) - M_E \cdot a(t)$$

$F(t)$ is given by;

$$F(t) = A \cdot (p_1(t) - p_3(t))$$

In the initial phase of the process, during the shock load, p_1 is not representative of the pressure on the whole slab. So, at this stage $F(t)$ cannot be determined correctly.

For $a(t)$, the acceleration of the first mode is used, because the modes can be treated separately. The third mode is not of interest, because it damps out.

M_E is given by:

$$M_E = KLM \cdot M = 207 \text{ kg}$$

By relating the resistance to the deformation of mode 1, the resistance-deformation curve is obtained, from which the ultimate deformation can be read.

REPORT DOCUMENTATION PAGE

(MOD-NL)

1. DEFENCE REPORT NO. (MOD-NL) TD98-0078	2. RECIPIENT'S ACCESSION NO.	3. PERFORMING ORGANIZATION REPORT NO. PML 1998-A38
4. PROJECT/TASK/WORK UNIT NO. 224496021	5. CONTRACT NO. A96D449	6. REPORT DATE December 1998
7. NUMBER OF PAGES 64 (incl. 4 annexes, excl. RDP & distribution list)	8. NUMBER OF REFERENCES 7	9. TYPE OF REPORT AND DATES COVERED Final
10. TITLE AND SUBTITLE Dynamic deformation capacity of reinforced concrete. Phase 5: influence of lacing reinforcement		
11. AUTHOR(S) J.C.A.M. van Doormaal S. Caron		
12. PERFORMING ORGANIZATION NAME(S) AND ADDRESS(ES) TNO Prins Maurits Laboratory, P.O. Box 45, 2280 AA Rijswijk, The Netherlands Lange Kleiweg 137, Rijswijk, The Netherlands		
13. SPONSORING AGENCY NAME(S) AND ADDRESS(ES) MOD-NL/DWOO, P.O. Box 20701, 2500 ES The Hague, The Netherlands		
14. SUPPLEMENTARY NOTES The classification designation Ongerubriceerd is equivalent to Unclassified.		
15. ABSTRACT (MAXIMUM 200 WORDS (1044 BYTE)) On behalf of MOD-NL/DWOO/HWO-CO blast tests were performed on simply supported reinforced concrete slabs. The resistance-deformation curves of the slabs were determined. From these curves, the deformation capacity of the slabs has been read. It was observed that the diameter of the longitudinal reinforcement has a considerable influence on the deformation capacity of the slabs and that it can change the failure mode. Concerning lacing, it was observed that it can only improve the deformation capacity if without it the slab would have failed due to buckling of the compression reinforcement. Two empirical relationships are found with which the deformation capacity of reinforced concrete slabs can be predicted. One is valid for failure in the compression zone, the other for failure in the tension zone.		
16. DESCRIPTORS Blast effects Concrete slabs Concretes Deformation Reinforced concrete		IDENTIFIERS Resistance
17a. SECURITY CLASSIFICATION (OF REPORT) Ongerubriceerd	17b. SECURITY CLASSIFICATION (OF PAGE) Ongerubriceerd	17c. SECURITY CLASSIFICATION (OF ABSTRACT) Ongerubriceerd
18. DISTRIBUTION AVAILABILITY STATEMENT Unlimited Distribution		17d. SECURITY CLASSIFICATION (OF TITLES) Ongerubriceerd

Distributielijst*

1	DWOO
2*	HWO-KL
3*	HWO-KLu
4*	HWO-KM
5	HWO-CO
6/8	DGW&T/CD/TB, Ir. D. Boon
9	DM&P TNO-DO
10*	DM&P TNO-DO, accountcoördinator CO
11*	TNO-FEL, Bibliotheek
12/14	Bibliotheek KMA
15*	Lid Instituuts Advies Raad PML Prof. Ir. J.A. Schot
16*	Lid Instituuts Advies Raad PML Prof. ir. K.F. Wakker
17*	Lid Instituuts Advies Raad PML BGen. Prof. J.M.J. Bosch
18*	Lid Instituuts Advies Raad PML Ir. A.H.P.M. Schaeken
19	TNO-PML, Directie; daarna reserve
20	TNO-PML, Hoofd Divisie Munitietechnologie en Explosieveiligheid Ir. P.A.O.G. Korting
21/23	TNO-PML, Divisie Munitietechnologie en Explosieveiligheid J.C.A.M. van Doormaal, S. Caron, Dr. J. Weerheijm
24	TNO-PML, Divisie Munitietechnologie en Explosieveiligheid, Groep Explosiepreventie en Bescherming, reserve
25	TNO-PML, Documentatie
26	TNO-PML, Archief

* De met een asterisk (*) gemerkte instanties/personen ontvangen uitsluitend de titelpagina, het managementuittreksel, de documentatiepagina en de distributielijst van het rapport.